Master's thesis

NTNU
Norwegian University of Science and Technology
Faculty of Information Technology and Electrical Engineering
Department of Electric Power Engineering

Jaume Martí Cascalló

Partial Discharge Testing and Prediction Modelling at High DC Voltage

Master's thesis in Electric Power Engineering

Supervisor: Frank Mauseth

July 2020

Manel Martí del Peral

NTNU
Norwegian University of Science and Technology

Jaume Martí Cascalló

Partial Discharge Testing and Prediction Modelling at High DC Voltage

Master's thesis in Electric Power Engineering
Supervisor: Frank Mauseth
July 2020

Norwegian University of Science and Technology
Faculty of Information Technology and Electrical Engineering
Department of Electric Power Engineering

NTNU
Norwegian University of
Science and Technology

Abstract

Internal partial discharges can be the cause of irreversible insulation degradation in High Voltage components, which can ultimately cause breakdown. Furthermore, they could become a condition indicator of the components, hinting a possible accelerated ageing due to other degradation mechanisms. Thus, acquiring a better understanding of the Partial Discharge mechanisms is of great interest. AC Partial Discharges have been widely studied, whereas DC Partial Discharges are a lesser-known phenomena.

The main purpose of this thesis is to provide a better understanding of the DC Partial Discharge behaviour. In order to achieve theoretical and practical comprehension, computer modelling and laboratory experiments were carried out during the present thesis. Two High Voltage DC Partial Discharge prediction models were developed and two different cavity sizes were compared for each model. The first model was based on the deterministic theory and the second model was created considering a stochastic starting electron generation rate. Both models were based on the ABC circuit model for internal partial discharges from voids in the insulation. The laboratory work consisted of improving the sensitivity of an existing Partial Discharge measuring set-up and performing Partial Discharge measurements in polyethylene terephthalate (PET) samples with different size disk-shaped cavities in the centre of the test object employing the improved set-up.

Concordance among the experiments, the High Voltage DC stochastic model and the theory for the time between discharges (tbd) behaviour was found. The time between discharges increases with decreasing cavity diameter due to smaller starting electron generation rate for flat cylindrical cavity geometry. The discharge magnitude was shown to have a similar trend as the time between discharges, thus with a decreasing cavity size the discharge magnitude increased. The temperature affected the time between discharges, increasing the tbd with decreasing temperature since a temperature reduction decreases the conductivity of the insulating material.

To conclude, a correlation between the cavity size, the time between discharges and the discharge magnitude is present. The relative behaviour can be successfully described by the High Voltage DC stochastic model as well as the stochastic theory and both envisage the observations in the laboratory. However, the correspondence between the stochastic model and the empirical data cannot be conclusively related.

Preface

This Master thesis is the denouement of the MSc. Electric Power Engineering at the Norwegian University of Science and Technology (NTNU). The present work has been carried out during the spring semester of 2020.

I want to express my gratitude to my supervisor Frank Mauseth for the help provided during the realization of this master thesis as well as the previous related work and to my co-supervisor Pål Keim Olsen for the enriching discussions, the help on the set-up improvement and the provided guidance through the whole project. A special mention to the people from the service lab and the workshop for their involvement, providing assistance, in my sometimes curious requests, for the laboratory work.

Trondheim, July 2020

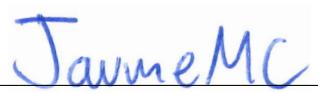

Jaume Martí Cascalló

Table of Contents

Chapter 1

Introduction

1.1 Background

Renewable energies are here to stay. There has been a rapid growth in this type of energy sources and they are becoming more prevalent in the energy production sector. The renewable energy par excellence in the past has been hydropower and it still is. Solar and wind energy are becoming more important and there has been a considerable increase in the amount of power plants for these type of energy sources. Wind power has gained importance in the electricity generation market and off-shore wind farms are becoming a great asset to expand this share. Off-shore wind farms present many advantages such as higher wind speed and larger-scale production than their on-shore counterparts, but they also encounter disadvantages, some of those being longer distance from shore and higher construction costs.

AC sub-sea power lines are currently the most used transmission method for Low to Medium Voltage. These type of power transmission finds its limitations for High Voltages (above 175 kV), high power or long distances. The feasibility of the AC cable systems for long distances, depending on the cable type and voltage, is estimated to be between 30 and 250 km [1]. The alternative to overcome these limitations is High Voltage DC cable transmission lines, which bestow higher load capacity due to the absence of capacitive currents and eddy currents, providing cables with almost negligible ascribed losses to distance. HVDC submarine cables are starting to become a viable solution given the amelioration of power electronics, the higher power capacity and a lower cost of the total system [1]. However, it needs to be considered the conversion from AC to HVDC would still leave some AC ripple due to the conversion, since it is extremely difficult to achieve a perfect HVDC waveform utilising power electronics with the current technology.

When performing the condition assessment of HVDC components, Partial Discharge is one of the degradations mechanisms to be considered. First, because it can cause irreversible degradation in the insulation and second, because it can underline other possible ageing mechanisms

that can, likewise, lead to breakdown. A greater understanding of Partial Discharges in DC and DC with AC combined [2] can become useful as it would benefit the analysis, diagnosis and better condition assessment for HVDC equipment.

1.2 Aim and Approach

The aim of this thesis was planned to be mostly practical, improving the sensitivity of an existing experimental set-up for Partial Discharge detection constructed by Olsen [2], validating the performance of the new set-up and performing DC Partial Discharge measurements to compare distinct features of the prepared samples, to better understand the DC Partial Discharge behaviour. Due to COVID-19, a more theoretical approach needed to be taken, therefore it was decided to generate prediction models for the HVDC Partial Discharge mechanism in a deterministic and a stochastic manner. Those models were coded utilising Matlab and the theory about DC Partial Discharges, providing a more thorough analytical approach. After some weeks of uncertainty, the laboratory work was allowed again, therefore the validation of the new test set-up and experiments for two of the initially planned types of samples were able to be performed.

In order to diminish the parameters affecting the Partial Discharge phenomena, customised PET samples with various cavity sizes were prepared, solely varying the cavity diameter. This would provide a type of sample, in combination with the set-up, where the nature of DC Partial Discharges in a single air cavity can be studied.

The main Partial Discharge parameters under High Voltage DC analysed in the present work at different temperatures are:

- The time between discharges.
- The discharge magnitude.
- The time between discharges ratio between a flat cavity with 2 mm diameter and a flat cavity with 6 mm diameter.
- The discharge magnitude ratio between a flat cavity with 2 mm diameter and a flat cavity with 2 mm diameter.
- The overall relative trend between the different cavities employing the time between discharges and the discharge magnitude for both cavity types.

1.3 Structure of the thesis

In Chapter 1 a brief presentation of the thesis is provided. In Chapter 2 the theoretical background needed to understand and analyse the experiments is presented. Thereafter, in Chapter 3 the High Voltage Partial Discharge prediction models are depicted and in Chapter 4 the experimental set-up is presented. Next, in Chapter 5 the analysis of the prediction models is conducted. Then, in Chapter 6 the results extracted from the experimental work are presented and in Chapter 7 the discussion of the analysed data is provided. To finish, in Chapter 8 the conclusions are formulated and further work is suggested in Chapter 9. Appendices with the Matlab code for the High Voltage DC Partial Discharge prediction models can be found at the end of this thesis.

Chapter 2

Partial Discharge Theory

As a prelude of this thesis, the author's specialisation project [3], where theoretical background was regarding the same subject, was performed. Therefore, some topics are addressed more extensively in the specialisation project. For this chapter, a more in-depth approach was taken on the subject of DC Partial Discharges.

2.1 Partial Discharges

The main ageing mechanisms in high voltage equipment are thermal ageing (produced by thermal stresses), mechanical ageing (produced by mechanical forces) and electrical stresses [4]. Regarding electrical stresses, high electric fields occurring in the weaker parts of the insulation favour the appearance of Partial Discharges, which can be an indicator of a defect in the insulation that can evolve until a breakdown develops. A local increase of temperature and chemical processes can derive from those mentioned phenomena and can also contribute to the deterioration of the insulation material [4].

According to IEC standard 60270, Partial Discharges (PD) are described as "a localized electrical discharge that only partially bridges the insulation between conductors and which can or cannot occur adjacent to a conductor" [5].

During the specialisation project, a more in-detail theoretical approach between AC and DC Partial Discharges was taken. One of the important outcomes was described by Pihera et al. [6], among others, that concluded the discharge magnitude in DC PD is smaller than for the AC case, which make DC Partial Discharges discharges more difficult to measure and Fromm [7], within his extensive work, studied the time between discharges (tbd) under DC and AC voltage and concluded that the tbd is considerably longer for DC than for AC.

2.1.1 Types of Partial Discharges

To acquire a better understanding about the master thesis topic, previous work was carried out in the specialisation project [3]. During the realization of the master thesis, no new relevant information on the types of Partial Discharges was found, therefore the presentation from the author's previous work [3] is presented below:

"The official partial discharge definition is a broad description that can be of different natures, which consequently have distinct behaviour even though they belong to the same category. Kao [8] and E. Kuffel et al. [9], among many others, have distinguished different main groups of Partial Discharges depending on their distinct features.

- Corona discharges are those that occur on the tips of a conductive material due to a concentrated electric field on the region. Corona discharges can be audible and even visible if the environmental conditions allow it.

- Surface discharges are discharges that occur at the surface of a dielectric material. Some of the reasons for that to occur can be the presence of impurities in the surface insulator that provides an electric field enhancement in that region or it also can be due to external agents as dust or dirt.

- Internal discharges manifest inside the dielectric material as a result of manufacturing impurities or by internal ageing of the dielectric material that can lead to internal defects.

- Electrical treeing is a combination of surface and internal discharges that has distinctive characteristics as it can develop through the dielectric material and has a tree-shape appearance when being created [8]."

2.2 DC electric field

The DC electric field is formed by two components and is described by Fromm [7] as

$$E_{DC} = E_{\epsilon} + E_{\rho} \tag{2.1}$$

where the component E_{ϵ} is determined by the permittivity distribution, as in an AC field, and it is initially dominant when a DC voltage is applied to the insulation. The component E_{ρ} is determined by the conductivity and builds up with time until it becomes the dominating term of the DC electric field (see Figure 2.1) [7].

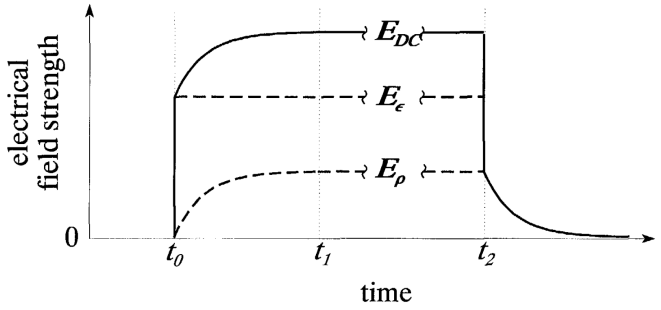

Figure 2.1: Different field situations at DC voltage. At $t = t_0$ a voltage V_0 is applied to the insulator. At $t = t_1$ the steady state DC field is reached. At $t = t_2$ the voltage is switched off. From Fromm [7].

The necessary time for the space charges to accumulate is usually much longer than the time required for the DC voltage to be applied, therefore at the moment of applying the voltage, E_ρ can be neglected [7].

$$E_{DC}\,(t_0) = E_\epsilon \tag{2.2}$$

After a certain time t_1, the space charge accumulation is completed and the DC steady-state is achieved. Then the E_{DC} behaviour would be determined by the conductivity [7]:

$$E_{DC}\,(t > t_1) = E_\rho \tag{2.3}$$

In summary, when applying a DC voltage to an insulator, there would be a space charge build-up time during which, the material would behave depending on the permittivity, and when the charge build-up in the insulation is completed, the conductivity would determine the demeanour of the insulation.

2.3 Paschen curve for air

The Paschen curve for air provides the minimum breakdown voltage depending on the pressure and the height of the void [4]. Many studies have been carried out on the breakdown voltage behaviour for various gap sizes and different insulating materials. No significant differences were found when comparing the results with the tests performed using equivalent gap spaces with metallic electrodes [10]. For this thesis it is going to be assumed that V_{Pasch} is the lower threshold voltage where PD can occur.

The Paschen voltage (V_{Pasch}) is is going to be calculated using the following equation from [4]

$$V_{Pasch} = 2420 \cdot p \cdot h + 2080 \cdot \sqrt{p \cdot h} \tag{2.4}$$

where the pressure p is in $[bar]$ and the height of the cavity h is in $[mm]$, with the resulting Paschen voltage V_{Pasch} in $[V]$.

2.4 Internal discharges in solid dielectrics under high DC voltage

When an insulating material with an internal cavity is subjected to an electric field, the stresses of the insulator are not going to be distributed evenly. In the cavity, since the permittivity and the conductivity are different from the insulating material, the stresses will also differ. When an electric field is applied to the insulation, the highest electric field will be present in the cavity, where Partial Discharges are more likely to develop [4]. There are two criteria that need to be fulfilled in order for Partial Discharges to develop. The first criterion is that a starting electron has to be present in the cavity. The second criterion is that the voltage across the cavity has to be over the Paschen voltage [7]. This voltage across the cavity can be called Partial Discharge Inception Voltage (PDIV) or ignition voltage (V_i). If the cavity size is considered to be constant, this two voltages can be associated to electric fields. For homogeneous electric fields and a constant cavity height, the electric field can be related to the voltage as

$$E = \frac{V}{h} \tag{2.5}$$

where V is the voltage across the cavity and h is the height of the cavity (see Figure 2.2).

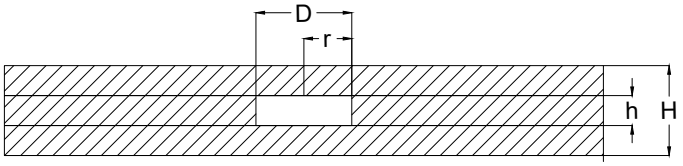

Figure 2.2: Solid dielectric material with a cylindrical cavity cross-section.

When the second criterion is expressed in terms of electric fields, the following needs to be fulfilled:

$$E_{PDIV} \geq E_{Pasch} \tag{2.6}$$

An explanation of the DC electric fields' behaviour is presented below, in comparison with AC fields. Initially, a virgin sample with a cavity, not exposed to any voltage, has to be assumed.

The first time a voltage is applied to the sample, it would create a charge distribution. To make the explanation more fathomable, before all else, a positive half-cycle voltage for AC and a positive DC voltage would be assumed. In this first electric field distribution the electric fields for AC and DC are going to be presupposed to have the same direction, but governed by different magnitudes. The AC electric field is governed by the permittivity, and the DC electric field is governed by the conductivity. If the electrodes' electric field is supposed to go from the cathode to the anode, the insulation electric field and the cavity electric field would have initially the same direction.

When an AC voltage is applied, the polarity of the electrons changes every half cycle, and due to the permittivity of the material, the electric field in the insulation would be opposing the electric field of the electrodes, generating a high electric field difference between the electrodes and the insulating material. The location in the insulation where the electric field would be the highest is inside the cavity. A discharge across the cavity is likely to develop if an electron is present and if E_{PDIV} inside the cavity is reached. A half-cycle later, the electrodes' electric field will change direction and the electric field in the cavity would be opposing it due to permittivity, that makes this change of polarity in the insulation slower than the one for the electrodes. If a discharge happened in the previous half cycle, a pool of electrons is likely to be present for the following half cycle.

When a DC voltage is applied, the field direction in the electrodes and the material will continue to have the same direction. If an electron in the cavity is present and the E_{PDIV} is reached inside the void, a partial discharge will occur, creating an opposing electric field to the electrodes' electric field. After some time, the electric field generated by the electrodes in the cavity and the electric field developed inside the cavity due to the discharges (one being of opposite direction to the other) will result in an overall electric field lower than E_{PDIV}, therefore the discharges will cease. The electric field in the void will slowly dissipate via conduction through the insulator until the overall electric field becomes higher than E_{PDIV} and another discharge can develop. The speed dissipation would depend on the material conductivity. In order for the next discharge to develop In contrast to the AC case, no pool of electrons is present due to the change of polarity, thus a starting electron needs to come stochastically into being (see section 2.4.1).

Two discharge mechanisms can occur in an air gap: Townsend and streamer discharge mechanism. These two phenomena were studied by Morshuis [11] for AC and for DC by Fromm [7]. In the specialisation project [3] previous to this master thesis, a more detailed explanation of both mechanisms was conducted.

The different characteristics of both mechanisms are described in Table 2.1 by Fromm [7].

Table 2.1: Properties of the different discharge types. From Fromm [7].

Townsend-like discharges	streamer-like discharges
• small overvoltage (few volts) • small current amplitude • duration proportional to gap height • covers large part of the void surface • residual voltage close to minimal breakdown voltage	• large overvoltage • large current amplitude • short duration • covers a fraction of the void surface • residual voltage close to zero

According to Fromm [7], the dominant discharge type for a polymeric insulation with a single cavity is the Townsend discharge mechanism, besides, when a discharge has a Townsend behaviour, it can be considered the residual voltage after a discharge to be similar to the Paschen voltage, thus $V_r \approx V_{Paschen}$. For this thesis it is going to be assumed the discharges across the cavity have a Townsend behaviour and that $V_r \cong V_{Paschen}$.

2.4.1 Electron generation mechanisms

The electron generation mechanism for insulation with a simple cavity is the sum of two procedures, volume generation (N_{vg}) and surface emission (N_{se}) [12].

$$N_{egm} = N_{vg} + N_{se} \tag{2.7}$$

2.4.1.1 Volume generation

Niemeyer [12] mentions two types of volume generation, which are radiative gas ionization by energetic photons (PI) and field detachment of electrons from negative ions (FD). These two processes are mainly dependent on the type of gas and the electric field [12].

2.4.1.2 Surface emission

In order to produce a starting electron from the surface, Niemeyer [12] describes four mechanisms. Those mechanisms are detrapping of electrons from traps at the insulation surface (DT), surface photo effect (PE), ion impact (II) and field emission from cathodic conductors [12].

For spherical cavities, the surface-to-volume ratio is small, therefore the volume generation mechanisms are the predominating processes (specially gas ionization) [12]. For flat cavities, since the surface-to-volume ratio increases substantially, the surface emission is dominating over the volume emission [13].

2.4.2 ABC circuit model for cylindrical cavities in a dielectric material

In order to analyse Partial Discharge measurements from a theoretical point of view, the ABC equivalent circuit for cylindrical cavities in a dielectric material is utilised [4]. A more extensive explanation of the ABC circuit is carried out in the author's specialisation project [3]. The ABC circuit from Figure 2.3 is an electrical approximation of the insulation material with a single air cavity properties in terms of electrical parameters where R_c and C_c represent the impedance across the cavity, R_b and C_b represent the impedance of the insulation in series with the cavity and R_a and C_a represent the rest of the impedance in parallel.

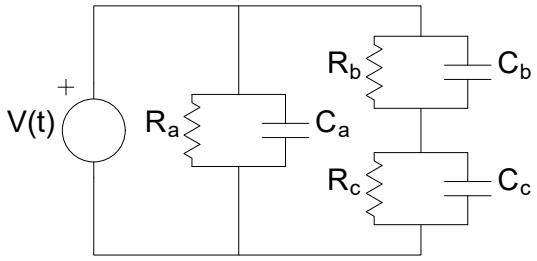

Figure 2.3: ABC circuit diagram for a single cavity in a dielectric material.

From Figure 2.3, C_b represents the capacitance in series with the cavity and is calculated as

$$C_b = \epsilon_{r_b} \cdot \epsilon_0 \cdot \frac{A}{H - h} \tag{2.8}$$

C_c represents the capacitance of the cavity and is calculated as

$$C_c = \epsilon_{r_c} \cdot \epsilon_0 \cdot \frac{A}{h} \tag{2.9}$$

C_b represents the resistance in series with the cavity and is calculated as

$$R_b = \rho_b \cdot \frac{H - h}{A} \tag{2.10}$$

C_c represents the resistance in the cavity and is calculated as

$$R_c = \rho_c \cdot \frac{h}{A} \tag{2.11}$$

where A is the area of the cavity, H is the height of the insulation material and h is the height of the cavity (see Figure 2.2). For this thesis the cavities are going to be considered cylindrical

with a great area-to-volume ratio, describing a flat cavity geometry. The area of the top surface of the cavity is described as

$$A = \pi \cdot r^2 \tag{2.12}$$

After a Partial Discharge is developed in the void, the voltage across the test object will be re-established by a transient current from the external circuit, which is associated to a charge, defined as apparent charge [4]. From the ABC circuit, the apparent charge can be extracted as

$$q_a \approx C_b \cdot \Delta V_c \tag{2.13}$$

where ΔV_c is the voltage drop in the cavity when a discharge occurs in the void. It can be observed the magnitude of the discharge only depends on C_b and ΔV_c. In order to obtain a more detailed review on the apparent charge see [3] and [4], where the mathematical approach to obtain eq. 2.13 can be found.

2.4.3 System time constant

The system time constant is defined by the properties of the insulation and the cavity. It can be calculated using the ABC equivalent circuit. According to Fromm [7], the system time constant is defined by

$$\tau_s = \frac{(R_b \cdot R_c) \cdot (C_b + C_c)}{R_b + R_c} \tag{2.14}$$

2.4.4 Evolution of the DC voltage with time

The derivative of the voltage in respect of the time $\left(\frac{dV}{dt}\right)$ determines how fast the voltage increases with time. It is dependent on the time constant of the system (τ_s), the voltage across the cavity if no discharge occurs (V_{con}) and the residual voltage after a discharge has occurred (V_r). Fromm [7] and Devins [14], among many others, have shown that the voltage steepness for DC is several orders of magnitude smaller than for AC.

Fromm [7] defines the voltage across the cavity as

$$V(t) = V_{con} - (V_{con} - V_r)\, exp\left(-\frac{t}{\tau_s}\right) \tag{2.15}$$

obtaining the first derivative

$$\frac{dV}{dt} = \frac{(V_{con} - V_r)}{\tau_s} \cdot exp\left(-\frac{t}{\tau_s}\right) \tag{2.16}$$

taking into account that $\frac{t}{\tau_s} \ll 1$, then $exp\left(-\frac{t}{\tau_s}\right) = 1$, providing a simplification for the $\frac{dV}{dt}$

$$\frac{dV}{dt} = \frac{(V_{con} - V_r)}{\tau_s} \tag{2.17}$$

where $V_r = V_{Paschen}$ when the discharge follows the Townsend mechanism characteristics (see section 2.4).

2.4.4.1 Influence of conductivity variation on the $\frac{dV}{dt}$

If the insulation material conductivity is considered to vary, this would have an effect on the system time constant, affecting the $\frac{dV}{dt}$. Conductivity is by definition the inverse of the resistivity.

$$\sigma = \frac{1}{\rho} \tag{2.18}$$

Assuming $R_c \gg R_b$ and constant C_b and C_c , τ_s can be described as

$$\tau_s = R_b \cdot (C_b + C_c) \tag{2.19}$$

from eq. 2.19, it can be extracted

$$\tau_s \propto R_b \tag{2.20}$$

from eq. 2.10 and eq. 2.18, R_b can be written as

$$R_b = \frac{1}{\sigma_b} \cdot \frac{H - h}{A} \tag{2.21}$$

then the relation between the characteristic time constant of the system (τ_s) and the conductivity of the insulating material (σ_b), when the rest of the parameters remain constant, would be

$$\tau_s \propto \frac{1}{\sigma_b} \tag{2.22}$$

and taking into account eq. 2.17, the relation between σ_b and $\frac{dV}{dt}$ is shown to be directly proportional

$$\frac{dV}{dt} \propto \sigma_b \tag{2.23}$$

2.5 Deterministic approach for high DC voltage

The requirement for Partial Discharges to occur from a deterministic point of view is the voltage across the cavity has to be equal to the Partial Discharge Inception Voltage (V_{PDIV}) [4]. In this section, the time between discharges, the discharge magnitude and the comparison between two cavities of different radii is going to be covered.

2.5.1 Time between discharges

The time when a discharge occurs is one of the values that can be obtained directly from the experiments. The time between discharges is proven to be more useful for Partial Discharge interpretation and it is easily obtainable from the registered time when discharges take place. The name is self-explanatory as it is defined as the elapsed time between two discharges. From Figure 2.4, when V_r is taken as the reference base threshold value, it can be extracted the voltage drop across the cavity is

$$\Delta V_c = \frac{dV}{dt} \cdot tbd \tag{2.24}$$

where tbd is the time between discharges

Rearranging from eq. 2.24, it can be observed that the time between discharges can be written as

$$tbd = \Delta V_c \cdot \left(\frac{dV}{dt}\right)^{-1} \tag{2.25}$$

and it only depends on the voltage drop across the cavity when a discharge occurs (ΔV_c) and $\frac{dV}{dt}$, which is going to be assumed to be constant for this thesis.

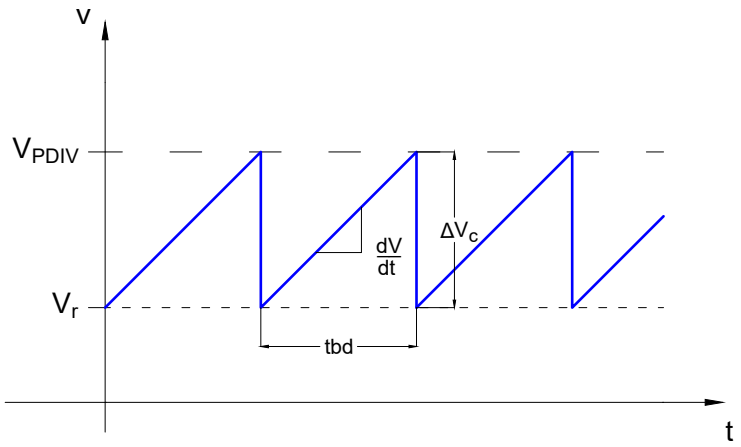

Figure 2.4: Voltage across the cavity at DC for the deterministic approach.

2.5.2 Discharge magnitude

From the ABC model (see eq. 2.13), it is shown that the discharge magnitude (q_a) is only dependent on the voltage drop in the cavity (ΔV_c) and C_b. Since C_b is constant because the cavity size for a given sample does not change, the discharge magnitude and ΔV_c are directly proportional. For the deterministic approach, q_a is calculated as

$$q_a = C_b \cdot \Delta V_c \tag{2.26}$$

2.5.3 Discharge magnitude and time between discharges correlation for two flat cavities of distinct radii

The assumptions in order to compare both cases are:

- Constant permittivity and conductivity.
- ΔV_c is the same for both cases (since all the discharges occur at the same voltage level the voltage drop across the cavity is going to be the same for every discharge).
- The height of the cylindrical cavity remains constant and $r_n = n \cdot r$, assuming n to be a positive integer different from 1.

First, the discharge magnitude is going to be analysed. The two discharge magnitudes to be compared are q_{a_r} (for the radius used as the reference) and $q_{a_{r_n}}$ (for the radius depending on $n \cdot r$).

Using eq. 2.8 and eq. 2.26, the following expressions can be extracted:

for the reference radius

$$q_{a_r} = C_{b_r} \cdot \Delta V_c$$

$$q_{a_r} = \epsilon \cdot \frac{\pi \cdot r^2}{H - h} \cdot \Delta V_c \tag{2.27}$$

for the radius depending on $n \cdot r$

$$q_{a_{rn}} = C_{b_{rn}} \cdot \Delta V_c$$

$$q_{a_{rn}} = \epsilon \cdot \frac{\pi \cdot r_n^2}{H - h} \cdot \Delta V_c \tag{2.28}$$

dividing eq. 2.28 by eq. 2.27

$$\frac{q_{a_{rn}}}{q_{a_r}} = \frac{\epsilon \cdot \frac{\pi \cdot r_n^2}{H-h} \cdot \Delta V_c}{\epsilon \cdot \frac{\pi \cdot r^2}{H-h} \cdot \Delta V_c} \tag{2.29}$$

substituting $r_n = n \cdot r$

$$\frac{q_{a_{rn}}}{q_{a_r}} = \frac{\epsilon \cdot \frac{\pi \cdot (n \cdot r)^2}{H-h} \cdot \Delta V_c}{\epsilon \cdot \frac{\pi \cdot r^2}{H-h} \cdot \Delta V_c} \tag{2.30}$$

simplifying eq. 2.30

$$\frac{q_{a_{rn}}}{q_{a_r}} = \frac{n^2}{1} \tag{2.31}$$

$$ratio_{q_a det} = \frac{n^2}{1}$$

From the analytical deterministic approach it can be extracted that the discharge magnitude ratio, when the cavity radius increases by n, the magnitude of the discharge will increase by n^2.

Hereafter, the tbd (time between discharges) is going to be analysed. The two time between discharges to be compared are tbd_r (for the radius used as the reference) and tbd_{r_n} (for the radius depending on $n \cdot r$). The assumptions mentioned at the beginning of the section are still applicable for this analysis.

Using eq. 2.25

$$tbd_r = \Delta V_{c_r} \cdot \left(\frac{dV}{dt}\right)^{-1} \tag{2.32}$$

$$tbd_{r_n} = \Delta V_{c_{r_n}} \cdot \left(\frac{dV}{dt}\right)^{-1} \tag{2.33}$$

considering $\frac{dV}{dt}$ to be constant and using eq. 2.32 and 2.33

$$\frac{tbd_{r_n}}{tbd_r} = \frac{\Delta V_{c_{r_n}}}{\Delta V_{c_r}} \tag{2.34}$$

as $\Delta V_{c_{r_n}} = \Delta V_{c_r}$

$$\frac{tbd_{r_n}}{tbd_r} = 1 \tag{2.35}$$

$$ratio_{tbd_{det}} = 1$$

From the analytical deterministic approach it is obtained the time between discharges becomes the same for cylindrical cavities with different radii, thus the time between discharges ratio is 1.

The relation between the discharge magnitude and the time between discharges for the same cavity can be described for the reference radius as

$$k_r = \left(\frac{q_{a,r}}{tbd_r}\right) \tag{2.36}$$

and for the radius directly proportional to the reference value as

$$k_{r_n} = \left(\frac{q_{a,r_n}}{tbd_{r_n}}\right) \tag{2.37}$$

Lastly, to obtain a general overview of the correlation between the discharge magnitudes and the time between discharges, the parameter k_{total} is calculated. Combining eq. 2.36 and eq. 2.37, k_{total} is shown to be

$$k_{total} = \frac{k_{r_n}}{k_r} = n^2 \tag{2.38}$$

In conclusion, it can be gathered the overall relation between two flat cavities of different diameter size in an insulation for the deterministic approach is n^2.

2.6 Stochastic approach for high DC voltage

The two criteria to be fulfilled for the stochastic method, in order for Partial Discharges to occur are the following:

The first criterion is that the voltage across the cavity has to be over the Paschen voltage (V_{Pasch}) [7]. This criterion is the same as in the deterministic approach (see sections 2.4 and 2.5).

The second criterion is the presence of an electron inside the cavity. In AC, due to its sinusoidal behaviour and its frequency, the electric field changes direction every half cycle, so it is likely that a pool of electrons from previous discharges is present and therefore PD are more likely to happen [13]. For DC, the electric field variability is almost non-existent when DC steady-state is reached. The DC steady state electric field builds up with time (see section 2.2) and has always the same direction (does not change as for the AC case), thus the pool of electrons is not present. Therefore, the electron generation has to happen in a different manner [7]. This electron generation mechanisms are explained in section 2.4.1.

If one of the criteria is not fulfilled, the discharge will not occur and the voltage across the cavity will build up to the voltage as if the insulation was void-free. The voltage across the cavity if no discharge occurs (V_{con}), is described by Fromm [7] as

$$V_{con} = V_0 \cdot \frac{R_c}{R_b + R_c} \tag{2.39}$$

where V_0 is the voltage applied to the test object.

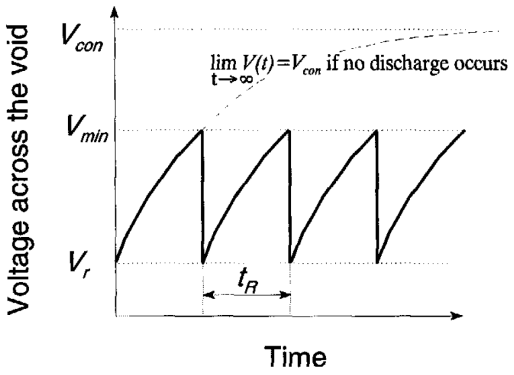

Figure 2.5: Voltage across the void for $V_i = V_{min}$, where V_i is the ignition voltage and V_{min} is the minimal breakdown voltage. From Fromm [7].

It is common that $R_c \gg R_b$ [4], thus for the present work it is going to be assumed

$$V_{con} = V_0 \tag{2.40}$$

2.6.1 Starting electron generation rate

The starting electron generation rate can be described as the frequency with which a starting electron is likely to be present. It is is mainly dependent on the electric field an temperature [13]. The expression that describes the starting electron generation rate is presented by Olsen as [13]

$$\dot{N}_s = N_0 \cdot exp\,(c_1 \cdot t_L) \cdot exp\,(c_2 \cdot T) \tag{2.41}$$

where T is temperature and t_L is the time lag (see section 2.6.2). The term $(c_2 \cdot T)$ is temperature dependent and the term $exp\,(c_1 \cdot t_L)$ is electric field dependent [13]. The parameters c_1 and c_2 are considered constants for this thesis, for further clarification on these values refer to [13]. Since $\frac{dV}{dt}$ is considered to be constant and ΔV_c is very small, consequently the electric field is also constant and $exp\,(c_1 \cdot t_L)$ term is then constant. The temperature for the theoretical approach is also considered constant, therefore $(c_2 \cdot T)$ remains as a constant. With the assumptions mentioned above, the starting electron generation rate is then going to be assumed constant.

From Olsen [13], the mean starting generation electron rate can be obtained as

$$N_{el} = \frac{1}{\tau_{el}} \tag{2.42}$$

where τ_{el} is the mean statistical waiting time [13].

To obtain the starting electron generation rate for the present work, Olsen's mean statistical waiting time was utilised [13]. Olsen's mean statistical waiting time [13] was for a determined cavity radius ($\tau_{el,r}$), thus the starting electron for different cavity sizes for the present work was found employing the starting generation electron rate per area

$$N_{el,A} = \frac{N_{el,r}}{A_r} \tag{2.43}$$

Ideally, the start electron generation rate for a different cavity size should be found experimentally, but for this thesis it was not possible to conduct these experiments, therefore the start electron generation rates are found using eq. 2.43 and the data provided by Olsen [13].

$$N_{el,new} = N_{el,A} \cdot A_{cavity} \tag{2.44}$$

2.6.2 Time lag

The time lag is described as the waiting time from when the Paschen voltage is surpassed until a discharge develops (see Figure 2.7). From Olsen [13], is given the time lag (t_L) depends on the starting electron generation rate. The probability function of the time lag depending on the starting electron generation rate is defined as [13]

$$pdf\left(t_{L_i}\right) = N_{el} \cdot exp\left(-N_{el} \cdot t_{L_i}\right) \tag{2.45}$$

and the cumulative distribution function is described as [13]

$$cdf\left(t_{L_i}\right) = 1 - exp\left(-N_{el} \cdot t_{L_i}\right) \tag{2.46}$$

From eq. 2.46, depending on N_{el}, the time lag cumulative distribution can vary substantially. In Figure 2.6, two cumulativa distribution functions for different N_{el} values are presented (for 1 mm and 3 mm radius).

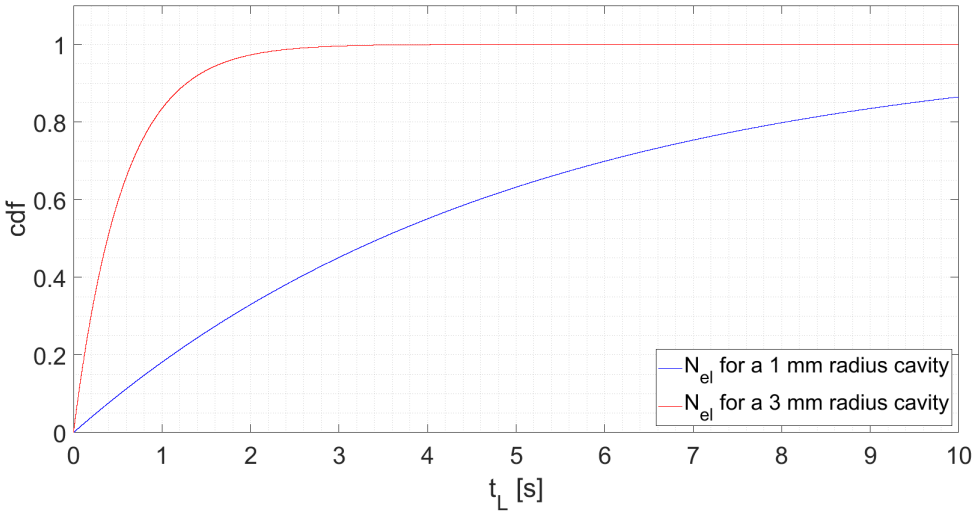

Figure 2.6: Cumulative distribution function depending on the time lag for a 1 mm radius cavity (blue) and a 3 mm radius cavity (red).

Using eq. 2.46, the time lag for each event can be calculated as a function of $cdf\ (t_{L_i})$

$$t_L = -\frac{ln\left[1 - cdf\ (t_{L_i})\right]}{N_{el}} \tag{2.47}$$

2.6.3 Voltage drop across the cavity

The voltage drop across the void (ΔV_c) is defined as the voltage drop experienced in the cavity when a discharge occurs. From Figure 2.7, ΔV_c can be described as the sum of two components: the voltage drop due to the time lag (ΔV_L) and the voltage drop due to the recovery time (ΔV_R).

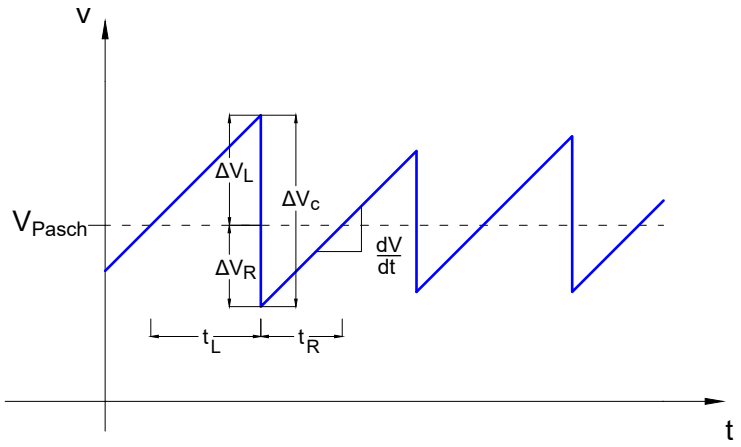

Figure 2.7: Voltage across the cavity at DC and the associated times for ΔV_L and ΔV_R for the stochastic approach.

From Figure 2.7 it can be extracted

$$\Delta V_R = \frac{dV}{dt} \cdot t_R \tag{2.48}$$

$$\Delta V_L = \frac{dV}{dt} \cdot t_L \tag{2.49}$$

$$\Delta V_c = \Delta V_L + \Delta V_R \tag{2.50}$$

inserting eq. 2.48 and eq. 2.49 into eq. 2.50

$$\Delta V_c = \frac{dV}{dt} \cdot t_L + \frac{dV}{dt} \cdot t_R \tag{2.51}$$

substituting t_R using eq. 2.58 (see section 2.6.4)

$$\Delta V_c = \frac{dV}{dt} \cdot t_L + \frac{dV}{dt} \cdot t_L \cdot (\alpha h - 1) \tag{2.52}$$

rearranging

$$\Delta V_c = \frac{dV}{dt} \cdot t_L + \frac{dV}{dt} \cdot t_L \cdot \alpha h - \frac{dV}{dt} \cdot t_L \tag{2.53}$$

$$\Delta V_c = \frac{dV}{dt} \cdot t_L \cdot \alpha h \tag{2.54}$$

using eq. 2.49

$$\Delta V_c = \alpha h \cdot \Delta V_L \tag{2.55}$$

From eq. 2.55, it can be observed ΔV_c is directly proportional to ΔV_L, which at the same time is directly proportional to the time lag (t_L).

2.6.4 Recovery time

The recovery time is described as the necessary time for the cavity to reach the Paschen voltage after a discharge has occurred across the void (see Figure 2.7). Devins [14] and Dissado [15] provided a relation between ΔV_R, ΔV_L and the proportionality factor (αh).

$$\frac{\Delta V_R}{\Delta V_L} = (\alpha h - 1) \tag{2.56}$$

In order to extract a relation between the time lag and the recovery time, eq. 2.48 and eq. 2.49 are employed

$$\frac{\frac{dV}{dt} \cdot t_R}{\frac{dV}{dt} \cdot t_L} = (\alpha h - 1) \tag{2.57}$$

as was stated in section 2.4.4, $\frac{dV}{dt}$ is considered constant. Simplifying eq. 2.57

$$t_R = t_L \cdot (\alpha h - 1) \tag{2.58}$$

The conclusion extracted from this section is the recovery time is proportional to the time lag. ΔV_R, which is dependent upon the recovery time, would also be a function of the time lag. From Devins [14], for very small overvoltages, a value of 9 is suggested for the proportionality factor, thus $\alpha h = 9$ will be used for the prediction models.

2.6.5 Time between discharges

The time between discharges (tbd) is described as the time elapsed between two discharges. In order to calculate the time between discharges, composed by the recovery time and the time lag, some considerations need to be done, those being the first time lag, the first discharge and the last recovery time are discarded. In Figure 2.8.a, is shown the time between discharges tbd_n is composed of the current recovery time and the time lag from the previous discharge. As a general expression, the time between discharges can be described as

$$tbd_n = t_{L_{n+1}} + t_{R_n} \tag{2.59}$$

where n is $\mathbb{Z}^+ > 0$.

In order to match the time between discharges to the discharge associated to its time

$$q_{a_i} = q_{a_{n+1}} \tag{2.60}$$

since the first discharge has been discarded.

When the first discharge is discarded (see Figure 2.8.b), the new discharge associated to the time between discharges tbd_n is q_{a_i}.

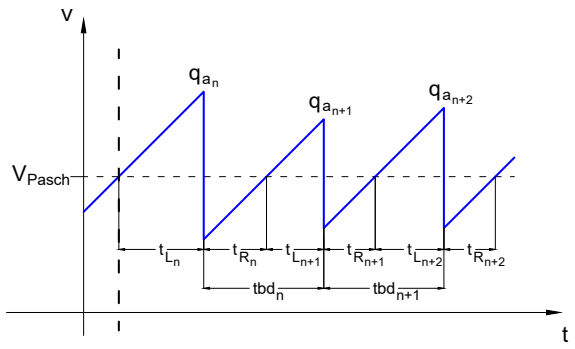

(a) Discharge and tbd relation before discarding the first discharge, the first time lag and the last recovery time.

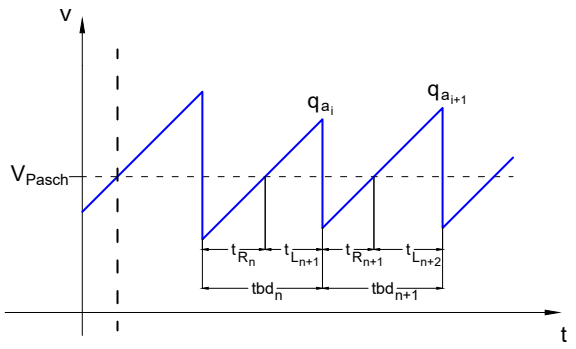

(b) Discharge and tbd relation after discarding the first discharge, the first time lag, the last recovery time and re-naming the discharges' sub-index.

Figure 2.8: Time between discharges composition based on the time lag (t_L) and the recovery time (t_R) associated to the discharges.

The average time between discharges $\left(\overline{tbd}\right)$ can be written as a function of the time lag. By definition, the average time between discharges is

$$\overline{tbd} = \bar{t}_L + \bar{t}_R \tag{2.61}$$

substituting the recovery time using eq. 2.58

$$\overline{tbd} = \bar{t}_L + \bar{t}_L \cdot (\alpha h - 1) \tag{2.62}$$

rearranging

$$\overline{tbd} = \bar{t}_L + \bar{t}_L \cdot \alpha h - \bar{t}_L \tag{2.63}$$

$$\overline{tbd} = \alpha h \cdot \bar{t}_L \tag{2.64}$$

The average time between discharges can be expressed as the proportionality factor times the average of the time lag, meaning there is a linear relation between the tbd and the t_L.

2.6.6 Discharge magnitude

The discharge magnitude extracted from the ABC model is dependent on C_b and ΔV_c, as shown in eq. 2.13. For the case of the stochastic approach, the voltage drop across the cavity is composed by the time lag (t_L), the proportionality factor (αh) and the cavity voltage variation with time $\left(\frac{dV}{dt}\right)$, as shown in eq. 2.54. Substituting ΔV_c (eq. 2.54) into eq. 2.13, the discharge magnitude for the stochastic method is then

$$q_a = C_b \cdot \alpha h \cdot \frac{dV}{dt} \cdot t_L \tag{2.65}$$

2.6.7 Discharge magnitude and time between discharges correlation for two flat cavities of distinct radii

In this section, the comparison between two different cavity sizes is going to be carried out. The method employed will be the previously presented stochastic approach. The assumptions and considerations to be done are the starting electron generation rate per area, the $\frac{dV}{dt}$, the relative permittivity and the conductivity are constant, the height of the cylindrical cavity remains constant and $r_n = n \cdot r$, assuming n to be a positive integer different from 1.

Preceding the discharge magnitude analysis, the time lag ratio will be examined and thereupon the discharge magnitude relation between the two different cavities is going to be illustrated. The parameters referring to the reference radius are going to be attributed the suffix r and the parameters referring to the radius depending on the reference one are going to be attributed the suffix r_n.

In section 2.6.2, it has been shown the time lag is dependent on N_{el}. The starting electron generation rate per area ($N_{el,A}$) is used to obtain the specific value for each cavity

$$N_{el} = N_{el,A} \cdot A \tag{2.66}$$

substituting the area from eq. 2.12

$$N_{el} = N_{el,A} \cdot \pi \cdot r^2 \tag{2.67}$$

Considering the reference cavity radius is r and the the other cavity has a $n \cdot r$ radius, the starting electron generation ratio correlation can be described as

$$\frac{N_{el,r_n}}{N_{el,r}} = \frac{N_{el,A} \cdot \pi \cdot (n \cdot r)^2}{N_{el,A} \cdot \pi \cdot r^2} \tag{2.68}$$

simplifying

$$\frac{N_{el,r_n}}{N_{el,r}} = \frac{n^2}{1} \tag{2.69}$$

The relation between the time lag and the starting electron generation rate, extracted from eq. 2.47, considering constant the rest of the parameters, can be deduced as

$$\bar{t}_L \propto \frac{1}{N_{el}} \tag{2.70}$$

Employing the correlation from eq. 2.47, the time lag ratio can be shown as

$$\frac{\bar{t}_{L,r_n}}{\bar{t}_{L,r}} \propto \frac{\frac{1}{N_{el,r_n}}}{\frac{1}{N_{el,r}}} \tag{2.71}$$

$$\frac{\bar{t}_{L,r_n}}{\bar{t}_{L,r}} \propto \frac{N_{el,r}}{N_{el,r_n}} = \frac{1}{n^2} \tag{2.72}$$

obtaining

$$\frac{\bar{t}_{L,r_n}}{\bar{t}_{L,r}} = \frac{1}{n^2} \tag{2.73}$$

Equation eq. 2.73 shows the ratio between both time lags to be of the form $\frac{1}{n^2}$. From eq. 2.64 it can be gathered

$$\bar{t}_L \propto \overline{tbd} \tag{2.74}$$

concluding the time between discharges ratio is

$$\frac{\overline{tbd}_{r_n}}{\overline{tbd}_r} = \frac{1}{n^2} \tag{2.75}$$

and has a correlation of $\frac{1}{n^2}$, similarly to the time lag.

From eq. 2.8, eq. 2.12 and eq. 2.65, the average discharge magnitude for the stochastic method can be written generally as

$$\overline{q}_a = \epsilon_{r_b} \cdot \epsilon_0 \cdot \frac{\pi \cdot r^2}{H - h} \cdot \frac{dV}{dt} \cdot \bar{t}_L \tag{2.76}$$

combining eq. 2.76 for two different radii it can be written

$$\frac{\overline{q}_{a,r_n}}{\overline{q}_{a,r}} = \frac{\epsilon_{r_b} \cdot \epsilon_0 \cdot \frac{\pi \cdot r_n^2}{H-h} \cdot \frac{dV}{dt} \cdot \overline{t}_{L,r_n}}{\epsilon_{r_b} \cdot \epsilon_0 \cdot \frac{\pi \cdot r^2}{H-h} \cdot \frac{dV}{dt} \cdot \overline{t}_{L,r}} \tag{2.77}$$

substituting the time lag ratio from eq. 2.73 and simplifying

$$\frac{\overline{q}_{a,r_n}}{\overline{q}_{a,r}} = \frac{\epsilon_{r_b} \cdot \epsilon_0 \cdot \frac{\pi \cdot r_n^2}{H-h} \cdot \frac{dV}{dt}}{\epsilon_{r_b} \cdot \epsilon_0 \cdot \frac{\pi \cdot r^2}{H-h} \cdot \frac{dV}{dt}} \cdot \frac{1}{n^2} \tag{2.78}$$

$$\frac{\overline{q}_{a,r_n}}{\overline{q}_{a,r}} = \frac{r_n^2}{r^2} \cdot \frac{1}{n^2} = \frac{n^2 \cdot r^2}{r^2} \cdot \frac{1}{n^2} \tag{2.79}$$

the ratio for the average discharge magnitude is expressed as

$$\frac{\overline{q}_{a,r_n}}{\overline{q}_{a,r}} = 1 \tag{2.80}$$

When considering the stochastic approach, the discharge magnitude for both cavity sizes, is proven to be the same. Therefore the ratio for the average discharge magnitude is 1.

In order to obtain the relation between both discharge magnitudes and time between discharges, from eq. 2.75 and eq. 2.80

$$\frac{\left(\frac{\overline{q}_{a,r_n}}{\overline{tbd}_{r_n}}\right)}{\left(\frac{\overline{q}_{a,r}}{\overline{tbd}_{r}}\right)} = n^2 \tag{2.81}$$

For simplification, the following substitutions were made:

$$k_{r_n} = \left(\frac{\overline{q}_{a,r_n}}{\overline{tbd}_{r_n}}\right) \tag{2.82}$$

and

$$k_r = \left(\frac{\overline{q}_{a,r}}{\overline{tbd}_{r}}\right) \tag{2.83}$$

To conclude, the overall correlation for the stochastic model parameters can be defined as

$$k_{total} = \frac{k_{r_n}}{k_r} = n^2 \tag{2.84}$$

The total ratio between two test objects with different cavity radii for the stochastic method has been shown to be of the form n^2, with the pertinent assumptions presented at the beginning of the section.

2.6.7.1 Conductivity dependency

For the stochastic approach it was considered to be of interest the effect of a variation in the conductivity for the test objects' insulating material. This can happen due to environmental effects (humidity, temperature, etc.). It can be shown, using eq. 2.23 and eq. 2.78, that k_{total} depending on the conductivity is

$$k_{total_{\sigma_b}} = n^2 \cdot \frac{\sigma_{b,r_n}}{\sigma_{b,r}} \tag{2.85}$$

as $k_{total} = n^2$

$$k_{total_{\sigma_b}} = k_{total} \cdot \frac{\sigma_{b,r_n}}{\sigma_{b,r}} \tag{2.86}$$

From eq. 2.86 it can be gathered that if the conductivity of the test object with the reference radius $(\sigma_{b,r})$ does not vary and the conductivity for the test object with bigger radius (σ_{b,r_n}) increases, $k_{total_{\sigma_b}}$ will increase. If the conductivity of the test object with the reference radius $(\sigma_{b,r})$ increases and the the conductivity for the test object with bigger radius remains constant (σ_{b,r_n}), $k_{total_{\sigma_b}}$ will behave inversely, and it will decrease.

Chapter 3

High Voltage DC Partial Discharge prediction models

Resulting from the exceptional circumstances of COVID-19, prediction modelling was decided to be introduced in this thesis. Two different models were considered to be of interest. The deterministic model, which follows the classic method considering an ignition voltage for discharges to occur. The second approach is the stochastic model, based mainly on the work from Devins [14], Fromm [7] and Olsen [13], where in order for discharges to occur, two conditions need to be fulfilled. It is important to be cognizant the models were constructed to provide relative estimations. The obtained predictions need to be interpreted with care, especially the stochastic model, as the relative estimation appears to be according to the theory, but due to the nature of the work, the total validity of the models could not have been supported with enough empirical data.

3.1 General conditions

Both models were designed with the number of discharges as an input to the model, to be able to adapt them when comparing with data obtained from laboratory experimentation. With the tests performed in the lab, the data obtained is the time discharges develop and the discharge magnitude. The time when discharges occur is post-treated to obtain the time between discharges for further analysis. For the purpose to achieve a resemblance between the models and the lab experiments, the discharge magnitude and the time between discharges are the desired output values provided by the models.

In order to create two comparable models, joint assumptions were presupposed; those being:

- Homogeneous electric fields.
- The geometry of the cavity is a cylinder with a high diameter-to-height ratio, leading to surface emission dominating over volume generation.
- Two different cavity radii (1 mm and 3 mm).
- The conductivity of the air is almost zero, therefore when a discharge develops the voltage drop only occurs across the cavity.
- Constant permittivity ($\epsilon_b = 3.1$ and $\epsilon_c = 1$) and PET conductivity ($\sigma_b = 1 \cdot 10^{-15}$) (it was not possible to conduct permittivity and conductivity tests, hence the values for the permittivity were obtained from [4] and the PET conductivity from the specialisation project [3]).
- Applied test voltage of 10 kV.
- The $\frac{dV}{dt}$ is calculated using eq. 2.17 and is considered to be constant.
- The values from the ABC circuit (C_b, C_c, R_b and R_c) were calculated using the equations shown in section 2.4.2.
- The models are only valid when the voltage across the cavity is over the Paschen voltage.
- The models simulate the DC steady state, assuming the space charges accumulation has been completed.

3.2 Stochastic model

In this section the procedure followed to code the stochastic model using the Matlab software will be explained. The code for this model can be found in section A.1 in the appendix.

Initially, C_b, C_c, R_b, R_c, τ_s, $V_{Pashcen}$ and $\frac{dV}{dt}$ are calculated.

Table 3.1: Calculated parameters used for both the stochastic and the deterministic prediction model.

Common parameters			
Variable	2 mm Ø cavity	6 mm Ø cavity	Units
C_b	$4.9275 \cdot 10^{-13}$	$4.4347 \cdot 10^{-12}$	[F]
C_c	$3.7088 \cdot 10^{-13}$	$3.3380 \cdot 10^{-12}$	[F]
R_b	$5.5704 \cdot 10^{16}$	$6.1894 \cdot 10^{15}$	[Ω]
R_c	$4.7746 \cdot 10^{50}$	$5.3052 \cdot 10^{49}$	[Ω]
τ_s	$4.8108 \cdot 10^{4}$	$4.8108 \cdot 10^{4}$	[s]
$V_{Paschen}$	757.2977	757.2977	[V]
$\frac{dV}{dt}$	0.1921	0.1921	$[V \cdot s^{-1}]$

The calculation of the time lag (see section 2.6.1) was the next step. In section 2.6.2 it is mentioned, the time lag is depending on the starting electron generation rate, which can be related to the mean statistical waiting time (τ_{el}) (see section 2.6.1). Olsen [13] determined experimentally the mean statistical waiting time for his work. From Olsen [13] is going to be considered $\tau_{el_{1mm}} = 5$ to obtain the starting electron generation rate for this thesis.

The cavity radius from Olsen [13] is 1 mm, so the starting electron generation rate is obtained for this cavity size.

$$N_{el,base} = \frac{1}{\tau_{el,base}} \tag{3.1}$$

In order to be able to extrapolate the starting electron generation rate to a different cavity size, the starting electron generation rate per area needs to be calculated.

$$N_{el,A} = \frac{N_{el,base}}{\pi \cdot r_{base}^2} \tag{3.2}$$

where $N_{el,A}$ units are $[electron \cdot s^{-1} \cdot m^{-2}]$.

Using eq. 2.43, the starting electron generation rate for the above mentioned cavities is found.

Table 3.2: Starting electron generation rate related to the cavity size.

Cavity diameter	Starting electron generation rate $[electron \cdot s^{-1}]$
2 mm	0.2
6 mm	1.8

All the procedures followed in order to design the stochastic model are performed for both cavity sizes (2 mm and 6 mm diameter). The number of events for the model is chosen to be 10 000 and it is done before the time lag calculation.

In order to calculate the time lag, eq. 2.47 is used. From figure 2.6, the relation between the cumulative distribution function and the time lag can be observed. In order to obtain the stochastic time lag, randomized values for the cumulative distribution function in the range of $(0, 1)$ are generated to provide a value for each event.

Thereafter, the recovery time (see section 2.6.4) and the magnitude of the discharge (see section 2.6.6) are computed from the cdf generated value. These values were associated to the time lag vector in order to keep track of the events occurring in the model.

To compare the simulation with the results obtained from the laboratory, the time between discharges and the discharge magnitude are extracted from the model. The moving average for the discharges and the time between discharges is plotted to help visualize the trends from the simulation (see Figure 3.1).

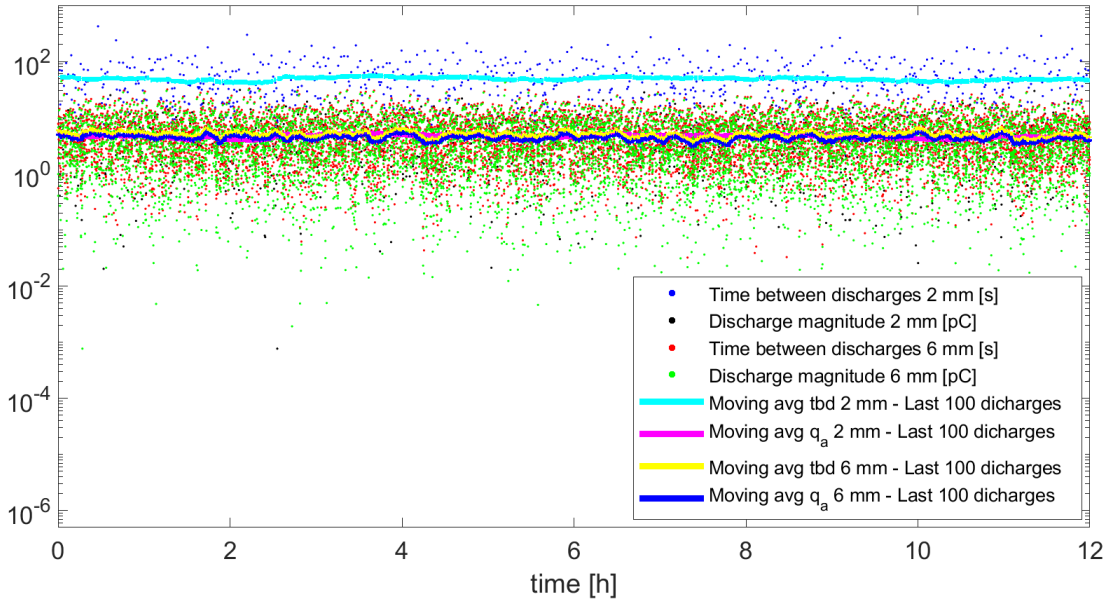

Figure 3.1: Discharge magnitude and time between discharges simulation for the stochastic model with 2 mm and 6 mm diameter cavities.

To be able to relate the deterministic model with the stochastic model, the average voltage drop across the 2 mm cavity diameter cavity $\left(\Delta\overline{V}_c = 8.6\ V\right)$ is calculated by eq. 2.54 and used as a constant for the deterministic model.

3.3 Deterministic model

The topic treated in this section is the deterministic prediction model. The code for this model can be found in section A.2 in the appendix.

The initial calculations were the same as for the stochastic model: C_b, C_c, R_b, R_c, τ_s, $V_{Pashcen}$ and $\frac{dV}{dt}$ (see table 3.1). Then, two parameters of interest were calculated, those being the discharge magnitude and the time between discharges. It is important to mention that to make the two models comparable, the average voltage drop across the 2 mm diameter cavity $\left(\Delta\overline{V}_c = 8.6\ V\right)$ from the stochastic model is employed. When performing the discharge magnitude calculation (see section 2.5.2), the equation is extracted from eq. 2.26. To calculate the time between discharges (see section 2.5.1), the equation is extracted from Figure 2.4, resulting in eq. 2.25. The evolution of the discharge magnitudes and the time between discharges for the deterministic model are shown in Figure 3.2.

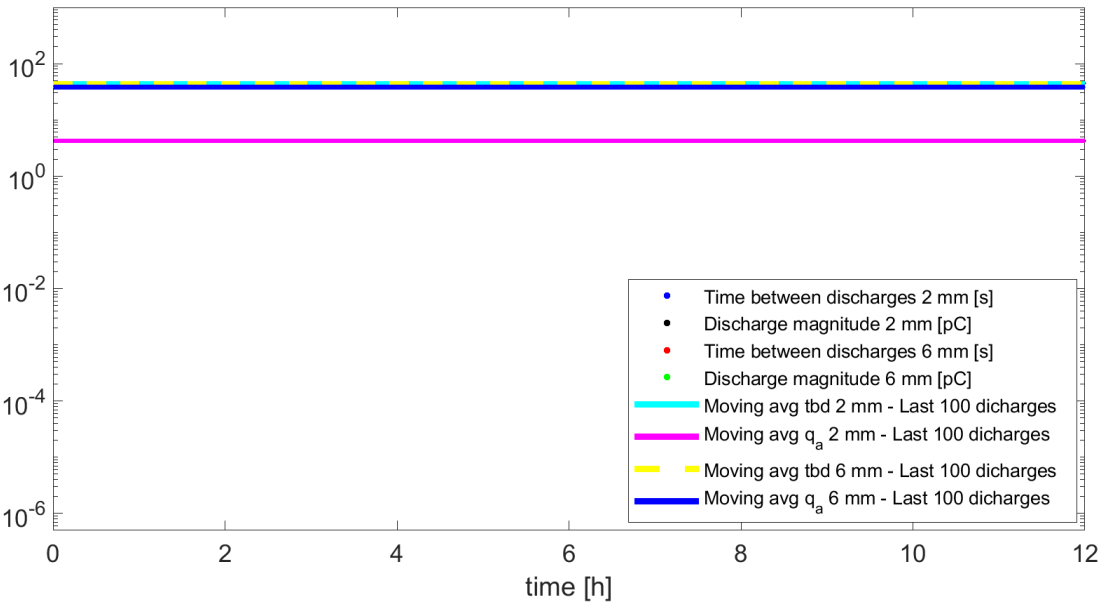

Figure 3.2: Discharge magnitude and time between discharges simulation for the deterministic model with 2 mm and 6 mm diameter cavities. The individual time between discharges and discharge magnitudes are displayed and they follow the same trend as the moving average, therefore can't be observed.

In contrast with the stochastic model, the discharge magnitude and the time between discharges calculations were straightforward since the two output values provided by the deterministic model were simpler to acquire. The values obtained for each discharge (q_a and tbd), for the

deterministic case, have both a constant value, meaning the simulations and moving averages have steady values of the same magnitude as the overall average. This trend can be observed in Figure 3.2 as all the discharge magnitudes, time between discharges and their averages follow the same constant values.

Chapter 4

Experimental set-up

This experimental set-up was built making the most of the set-up Olsen designed and constructed for his doctoral work [13]. Some changes were introduced to the initial set-up in order to adapt it to the purpose of this thesis. The set-up was comprised of three main ambits: The High Voltage circuit, the Partial Discharge measuring circuit and the heating circuit.

4.1 Set-up introduction

The set-up was initially designed for measuring Partial Discharges for DC with combined AC [2]. In order to measure Partial Discharges, the discharge currents have a low impedance path through the capacitor C_s, and R_s discharges the capacitances after the detection. This design is the standard for Partial Discharge detection circuit [2]. Considering the adaptability of this design, a buffer resistance R_d is connected in series with the DC source to block the AC current injection to the DC power supply and a buffer capacitance C_d is connected in series with the AC generation branch in order to block DC currents. C_d has a higher capacitance than C_s and the test object, to ensure the voltage drop occurs in the test cell. For a more in-depth explanation of the set-up for combined DC and high frequency AC voltage refer to [2].

For this thesis the AC branch was grounded. The buffering resistance R_d was kept in place and the buffering capacitance C_d was replaced from the initial 5.75 nF to a 5900 pF ceramic capacitor. For the coupling capacitor, the former 179 pF paper-oil capacitor was replaced by a 715 pF ceramic capacitor. The resistance R_s was maintained. Since the C_s's capacitance was increased and the ratio between the two capacitors was reduced, the measuring sensitivity of the system was increased. In series with C_s, an internal quadrupole Partial Discharge measuring system was connected in order to register the events (further explanation is conducted later on this chapter, see section 4.5).

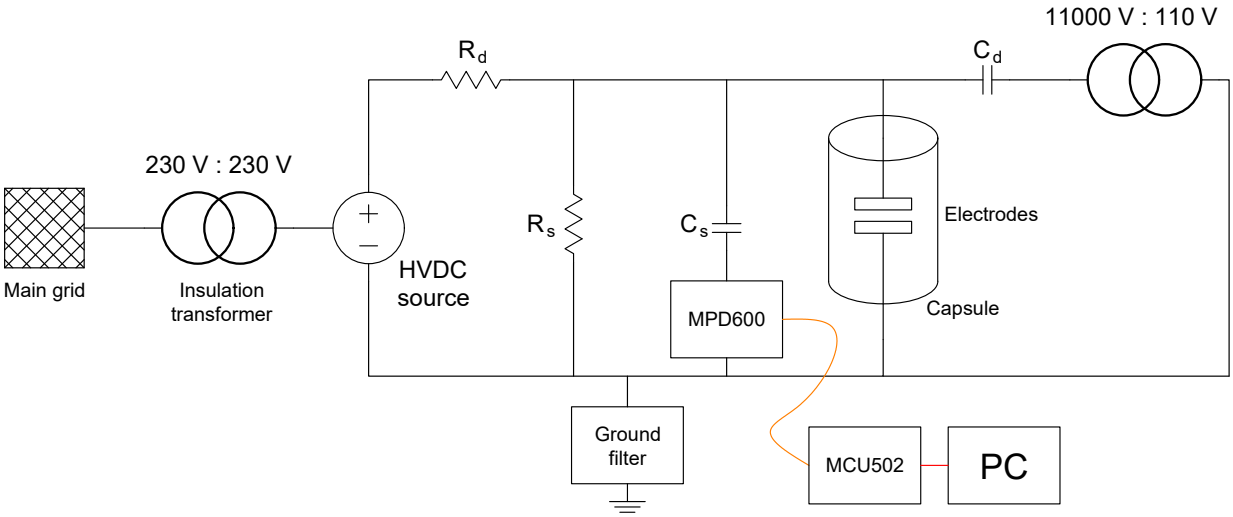

Figure 4.1: HVDC generation and Partial Discharge detection circuit.

4.2 Test samples

Three types of tests samples were used. The first sample type consisted of a 70 mm diameter and 0.25 mm height PET solid disk with no cavities. The two other types of samples had a "sandwich configuration", which consisted of three 70 mm diameter and 0.075 mm thickness PET sheets. The middle sheet had a cylindrical cavity in the center. These cavities had a 2 mm and 6 mm diameter respectively.

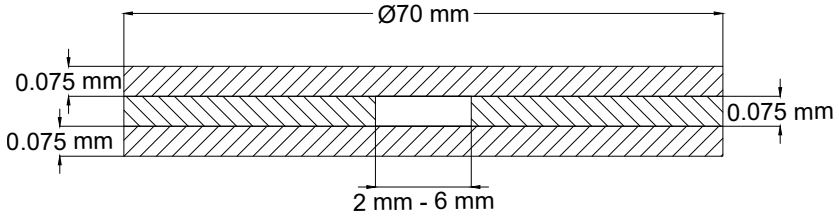

Figure 4.2: Test object structure's cross-section. Three PET sheets with cylindrical hole in the middle sheet.

In order to avoid the presence of air bubbles and oil leakage inside the samples during testing, the sheets were glued together along the outermost contour. During the gluing process, the samples were allocated in a hydraulic press at room temperature where the whole sample except the outer contour was subjected to high pressure in order to ensure air was only present in the cavity.

Table 4.1: Summary of the PET sample types

Sample thickness	Cavity diameter
0.25 mm	-
3 x 0.075 mm	2 mm
3 x 0.075 mm	6 mm

4.3 Test procedure

During the author's specialisation project, the proper functioning of the separate components and noise levels of the set-up, with $C_s = 179\ pF$ and $C_d = 5.75\ nF$ at room temperature, were measured and validated. For the master thesis, the noise evaluation for the heating circuit and the set-up with the new capacitors needed to be verified before proceeding to the main Partial Discharge measurements.

The tests were organised in the following manner:

- Heating circuit noise test.
- High Voltage circuit noise tests at room temperature with PET disk sample.
- System noise tests to ensure the correct functioning of the overall set-up with PET disk sample.
- Partial Discharge detection tests with samples of 2 mm and 6 mm cavities at different temperatures.

The Partial Discharge tests were complemented with prediction models developed in Matlab.

4.4 Equipment

The equipment employed for the three different circuits on the set-up are listed below.

4.4.1 High Voltage circuit

- FuG Elektronik GmbH ultra stable 35 kV - 4 mA High Voltage DC source [B02-0749].
- 500 $M\Omega$ and 100 $M\Omega$ High Voltage resistors.
- 179 pF oil-paper and 5.75 nF disk High Voltage capacitors.
- 715 pF and 5900 pF ceramic High Voltage capacitors.
- Test cell designed and constructed by Olsen [13].
- 230 V - 130 V / 1600 VA 60 Hz Ulveco isolation transformer [B01-0567].

- USB fibre optic cable to remotely control the HVDC power supply.
- TENMA 72-2540 programmable DC Power supply 30 V - 5 A [B02-0703] to provide power to the USB cable.
- ProVIL - GUI for FuG Power Supplies software.
- GF50 Power Diagnostix ground filter [I06-0565].

4.4.2 Partial Discharge measuring circuit

- OMICRON advanced Partial Discharge measurement system MPD 600 [H02-0195-03].
- OMICRON fibre-optic bus controller MCU 502 [H02-0195-02].
- Fibre optic cable to transfer the recorded data to the computer.
- OMICRON Software for MPD and MI.
- Mascot Type 719, 30 V - 1.5 A DC Power supply [B02-0422] to provide power to the MPD 600.

4.4.3 Heating circuit

- 34972A Agilent LXI Data Acquisiton / Switch unit [G05-0183].
- TENMA 72-2540, 30 V - 5 A programmable DC Power supply [B02-0701] to power the data acquisition unit.
- Transducer LKM 224 PT100, 0..150 $^{\circ}\mathrm{C}$ - 0..10 V.
- Heating coil designed and constructed by Olsen [13].
- Topaz Electronics line noise suppressing ultra-isolator transformer [B01-0391].
- Lübcke Vario variac type R54-260B, 260 V - 8 A power supply [B01-0371].
- BenchLink Data Logger 3 software.

All the recorded data from the PD measuring circuit and the cell temperature was stored in the computer for further analysis.

4.5 Set-up configuration

The assembly of the different circuits of the set-up is going to be explained in this section.

4.5.1 High Voltage circuit

The High Voltage circuit was composed of the FuG HVDC source connected in series with the resistor R_d. In parallel with the voltage source, the resistor R_s, the capacitor C_d, the capacitor C_s and the test cell were connected (see Figure 4.1). In order to prevent external noise, the HVDC source was connected to an isolation transformer to separate the system from the grid. To control the HVDC source remotely, the DC source was connected to the computer through a USB fibre optic cable. During the specialisation project [3], it was ensured the DC power supply did not provide any detectable noise to the system. A ground filter GF50 was connected to the common circuit grounding to prevent noise from the ground connection.

4.5.2 Partial Discharge measuring circuit

To register the events, the MPD 600 was connected in series with the coupling capacitor (C_s) to detect the discharge currents. Via fibre optics cable, the MPD 600 was connected to the MCU 502, which was connected to the PC via USB. In order to visualize and record the Partial Discharges, the OMICRON Software for MPD and MI was employed. To register the discharges, the frequency band with the minimum noise was chosen, the center frequency being 500 kHz with a Δf of 300 kHz. During the specialisation project [3] it was ensured the voltage sources did not introduce any detectable noise to the measuring circuit.

4.5.3 Heating circuit

For this thesis, the temperature of the oil was controlled by the heating circuit. The heating circuit was comprised of a metallic coil inside the test cell [13], connected to a Variac. The desired temperature was established by adjusting manually the power supplied by the Variac with the trial-error method. An isolation transformer was connected between the Variac and the grid to avoid noise generated from the main grid. To determine the oil temperature, the temperature sensor in the oil was connected to the PT 100 element that provided the information to the Datalogger, which transferred the data to the computer. The software used to record the temperature was the BenchLink Data Logger 3.

4.6 Verification of the experimental set-up

In this chapter, the process to obtain the final set-up for Partial Discharges detection tests is going to be developed. The planned work was to change the 179 pF paper-oil capacitor and the 5.75 nF disk capacitor from the previous set-up [3] for a 715 pF and 5900 pF ceramic

capacitor respectively. In order to ensure the proper functioning of the new set-up, noise tests after the substitution of individual components needed to be performed. For this set of tests the PET disk sample was used, since the goal was to ensure no discharges were occurring across the sample when evaluating the set-up. After every change done in the set-up, the system was calibrated before testing to ensure the rightness of the measurements.

4.6.1 Threshold

To ensure the well-functioning of the new capacitors, these were tested independently in a capacitance meter. Only one capacitor was substituted at a time in the set-up. The first change was to substitute the 179 pF paper-oil capacitor for the 5900 pF ceramic capacitor. After this action, a noise threshold measurement was conducted. In order to establish the minimum threshold for the new configuration, the HVDC source and the heating system were disconnected and the threshold was lowered until environmental noise was recorded. When the threshold had a value of 350 fC, constant environmental noise was measured. The threshold for the system was then set to 400 fC.

4.6.2 Heating circuit test

Initially, the thermal circuit needed to be adjusted to the desired temperature of 77 $^{\circ}\mathrm{C}$ as described in section 4.5.3. When the desired temperature was reached, a noise test with the HVDC source disconnected for 3 hours and then connected at 0 kV for 4 hours with the heating circuit connected for the whole 7 hours, to ensure no discharges were registered due to the heating circuit. After 7 hours of testing, only two discharges were registered. This concluded the heating circuit did not introduce noise to the system.

4.6.3 High Voltage circuit tests at room temperature

4.6.3.1 5 kV DC, $C_s = 5900\ pF$ - $C_d = 5.75\ nF$

After ensuring the heating circuit did not introduce noise to the system, the heating circuit was disconnected and the oiled cooled down from 77 $^{\circ}\mathrm{C}$ to room temperature (20 $^{\circ}\mathrm{C}$). When the oil was at room temperature, a 5 kV test was performed to observe the amount of discharges recorded at this stage. This test had a duration of 27 hours and the recorded discharges were 163.

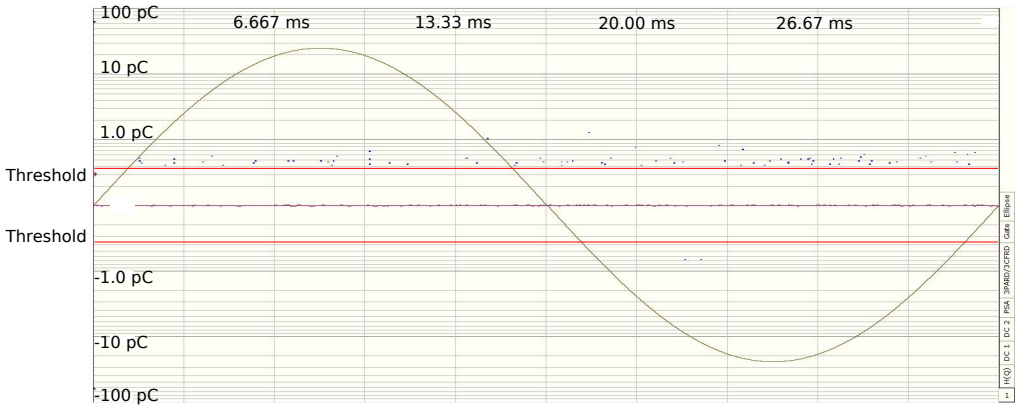

Figure 4.3: 5 kV DC test at room temperature with $C_s = 5900\ pF$ and $C_d = 5.75\ nF$ with the PET disk sample.

4.6.3.2 5 kV DC, $C_s = 715\ pF$ - $C_d = 5.75\ nF$

For this test, the 5900 pF capacitor was substituted by the 715 pF capacitor. The main objective of this test was to observe both new capacitors under the same circumstances to ensure a correct behaviour within the system. This test had a duration of 42 hours and 99 pulses were recorded.

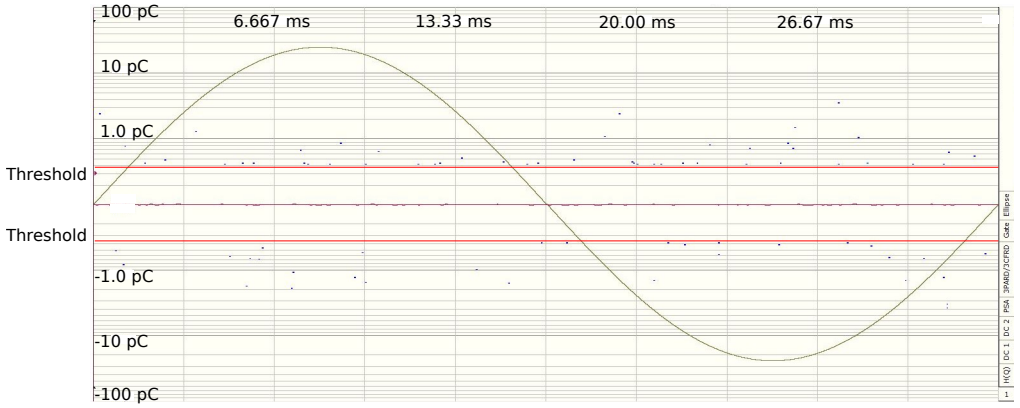

Figure 4.4: 5 kV DC test at room temperature with $C_s = 715\ pF$ and $C_d = 5.75\ nF$ with the PET disk sample.

4.6.4 Set-up tests at 77 °C

4.6.4.1 5 and 10 kV DC, $C_s = 715\ pF$ - $C_d = 5.75\ nF$

This tests were performed after the 715 pF installed capacitor at room temperature functioned properly and the heating system was also performing as expected. The aim for these tests was to observe the combination of both circuits operating at the same time. Two different voltages were tested (5 and 10 kV) with the oil temperature at 77 °C. The 5 kV test was performed for 24 hours and the 10 kV test for 17 hours. For both cases, the amount of discharges and the

discharge magnitudes were higher than expected, which meant there was a problem regarding the combination of both circuits.

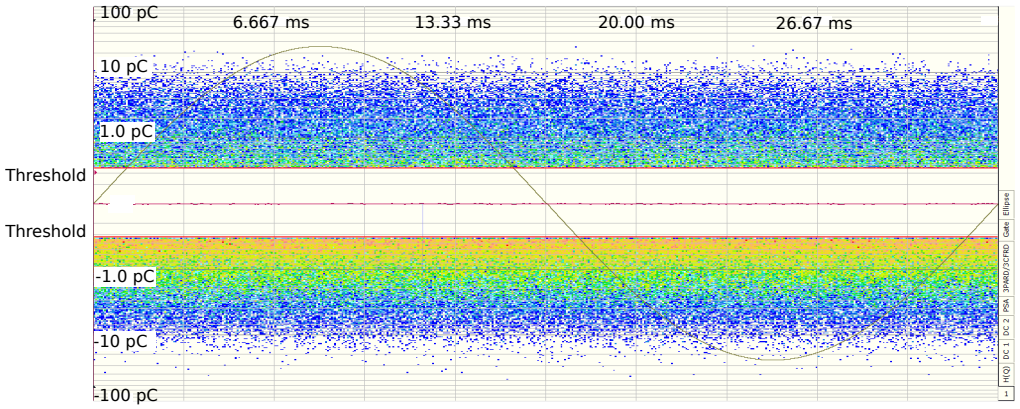

Figure 4.5: 5 kV DC test at 77 °C with $C_s = 715\ pF$ and $C_d = 5.75\ nF$ with the PET disk sample.

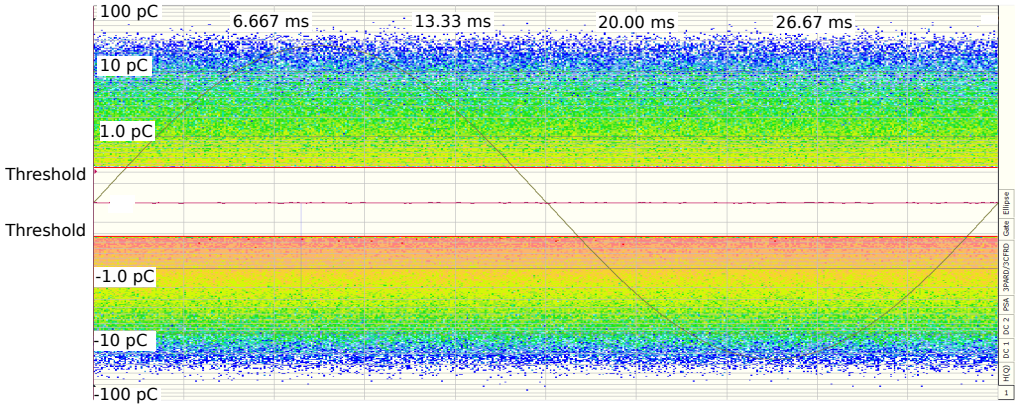

Figure 4.6: 10 kV DC test at 77 °C with $C_s = 715\ pF$ and $C_d = 5.75\ nF$ with the PET disk sample.

4.6.4.2 Troubleshooting

In order to solve the numerous amount of measured discharges, different capacitor combinations were mounted in the system to find what was the cause of such an abnormal behaviour, but the problem persisted. Finally, it was found that the bottom electrode connection, when the temperature of the system was increased, had an intermittent behaviour. Sometimes the connection was solid, and sometimes there was a bad connection. The intermittent connection could have been due to the different materials dilatation coefficient when temperature is increased. It was essential to ensure a solid connection of the bottom electrode before proceeding to further evaluation.

4.6.4.3 *10 kV DC,* $C_s = 179\ pF$ - $C_d = 5.75\ nF$

After the bottom electrode connection was fixed, the set-up's initial capacitors were installed. The reason to do so is that the initial set-up for the master thesis was evaluated during the specialisation project [3] and it was proven to be reliable at room temperature. The addition of the thermal circuit after troubleshooting was the only difference. The threshold was set to 600 fC [3] and the noise test was carried out. The test was performed during 40 hours and it can be observed in Figure 4.7 the recorded discharges were much lower and less abundant than before troubleshooting.

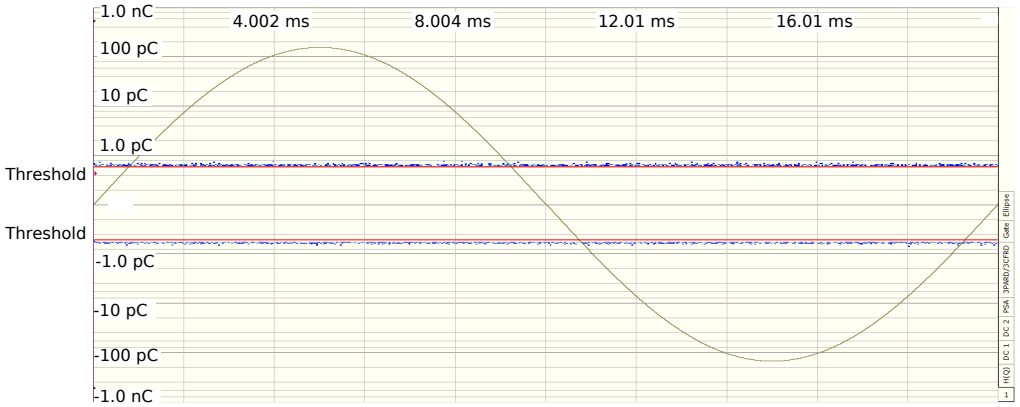

Figure 4.7: 10 kV DC test at 77 °C with $C_s = 179\ pF$ and $C_d = 5.75\ nF$ with the PET disk sample.

Chapter 5

Analysis of the prediction model results

In this chapter the ratios for the time between discharges and the discharge magnitude, along with the overall correlation for two different cavities for both models are going to be evaluated and compared with the theory (see section 2.5.3, where the theoretical approach for the deterministic model is treated, and section 2.6.7, where the theoretical approach for the stochastic model is presented).

For both models, the time between discharges ratio allows a better comprehension of the relation between two cavities with distinct diameter. For the 2 mm and 6 mm cavity diameter is defined as

$$ratio_{tbd} = \frac{\overline{tbd}_{6mm}}{\overline{tbd}_{2mm}} \tag{5.1}$$

The time between discharges ratio provides a quick understanding of the discharge magnitude relation between two cavities of different radii. For the 2 mm and 6 mm cavity diameter is described as

$$ratio_{q_a} = \frac{\overline{q_a}_{6mm}}{\overline{q_a}_{2mm}} \tag{5.2}$$

The correlation between the discharge magnitude and the time between discharges for the same cavity radius is defined as

$$k_r = \frac{\overline{q_a}_r}{\overline{tbd}_r} \tag{5.3}$$

for the 2 mm cavity diameter as

$$k_{2mm} = \frac{\overline{q_a}_{2mm}}{\overline{tbd}_{2mm}} \tag{5.4}$$

and as for the 6 mm cavity diameter.

$$k_{6mm} = \frac{\overline{q_a}_{6mm}}{\overline{tbd}_{6mm}} \tag{5.5}$$

To acquire a global understanding of the trend correlation behaviour between $q_{a_{2mm}}$, $q_{a_{6mm}}$, tbd_{2mm} and tbd_{6mm}, the calculation of k_{total}, which encompasses the four parameters, can be expressed as

$$k_{total} = \frac{k_{6mm}}{k_{2mm}} \tag{5.6}$$

5.1 Deterministic model

The deterministic model was chosen to have 10 000 events for the 2 mm diameter cavity and the same number of events for the 6 mm diameter cavity. With the aim to be able to calculate the time between discharges and the discharge magnitude ratios, the average values for the discharge magnitude for the 2 mm diameter cavity ($\overline{q_a}_{2mm}$), the time between discharges for the 2 mm diameter cavity ($\overline{tbd}_{2mm}$), the discharge magnitude for the 6 mm diameter cavity ($\overline{q_a}_{6mm}$) and the time between discharges for the 6 mm diameter cavity ($\overline{tbd}_{6mm}$) were calculated.

The time between discharges ratio for the deterministic model was calculated utilising eq. 5.1

$$ratio_{tbd} = 1$$

and the discharge magnitude ratio for the deterministic model by utilising eq. 5.2 was found to be

$$ratio_{q_a} = 9$$

From Figure 5.1, it can be observed the simulated ratios for the deterministic models with a moving average from the last 100 discharges maintains a constant trend through the whole simulation. The reason for this constant behaviour is the constant PDIV, as it will entail a constant time between discharges and a constant discharge magnitude. The model results are the expected from the theory (see section 2.5.3) where the $ratio_{tbd}$ and $ratio_{q_a}$ were calculated to have a value of 1 and 9 respectively.

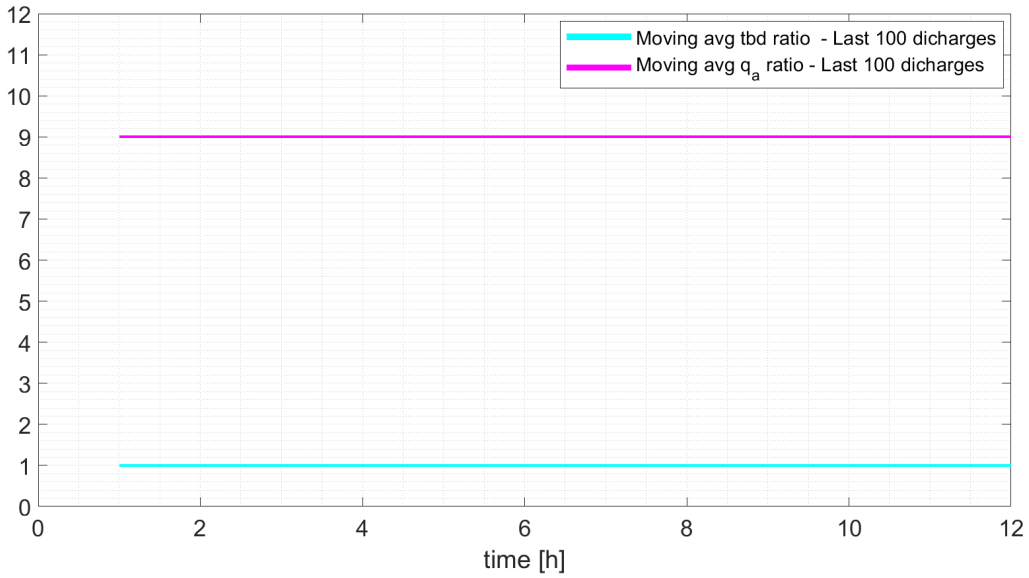

Figure 5.1: $ratio_{tbd}$ and $ratio_{q_a}$ with a moving average from the last 100 discharges for the deterministic model with 2 mm and 6 mm diameter cavities.

For the purpose of understanding the overall trend between both cavity sizes, the moving average of k_{total} was calculated using eq. 5.6

$$k_{total} = 9$$

In Figure 5.2, it can be gathered the value of the moving average for k_{total} of the last 100 discharges is constant at a value of 9 throughout the whole simulation, which is in concordance with the theoretical approach for the deterministic model (see section 2.5.3) where k_{total} has a value of 9.

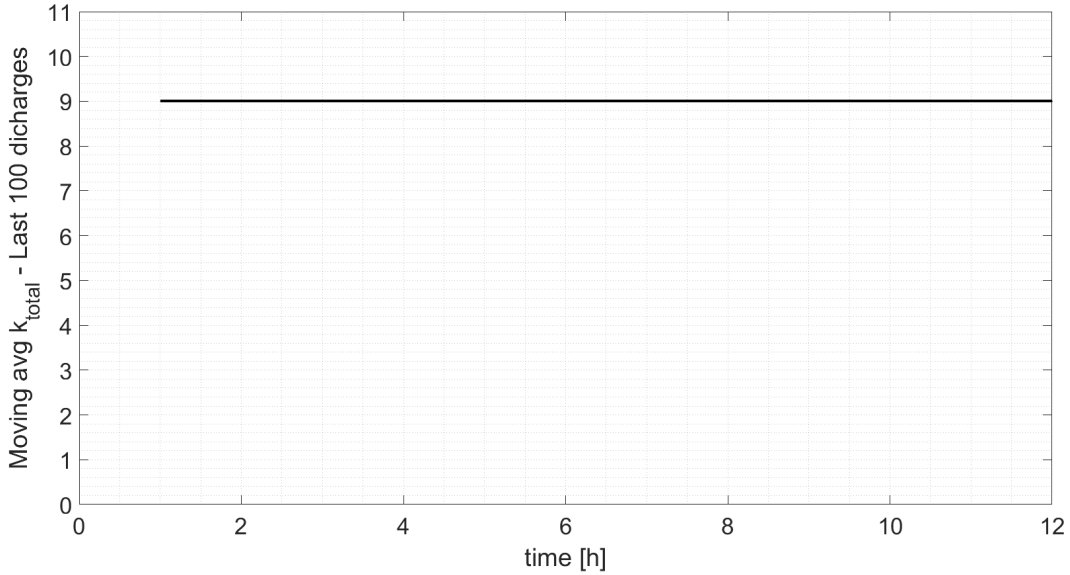

Figure 5.2: k_{total} with a moving average from the last 100 discharges for the deterministic model with 2 mm and 6 mm diameter cavities.

5.2 Stochastic model

The simulation for the stochastic model was performed with 10 000 events for both the 2 mm diameter cavity and the 6 mm diameter cavity. For all the magnitude of discharges and the time between discharges obtained for each cavity size, the average was calculated obtaining the values for the average discharge magnitude for the 2 mm diameter cavity ($\overline{q_a}_{2mm}$), the average time between discharges for the 2 mm diameter cavity $\left(\overline{tbd}_{2mm}\right)$, the average discharge magnitude for the 6 mm diameter cavity ($\overline{q_a}_{6mm}$) and the average time between discharges for the 6 mm diameter cavity $\left(\overline{tbd}_{6mm}\right)$.

Using eq. 5.1, the time between discharges ratio for the stochastic model was calculated

$$ratio_{tbd} = \frac{1}{9}$$

and using eq. 5.2, the discharge magnitude for the stochastic model was calculated

$$ratio_{q_a} = 1$$

It can be observed the results obtained from the simulation are in concordance with the theory (see section 2.6.7) where the $ratio_{tbd}$ has a value of $\frac{1}{9}$ and $ratio_{q_a}$ has a value of 1. In Figure 5.3 the representation of the discharge magnitude and time between discharges moving average from the last 100 discharges is displayed. It can be observed the parameters follow the expected value with slight oscillations due the stochastic variation of the curves caused by the starting

electron generation rate.

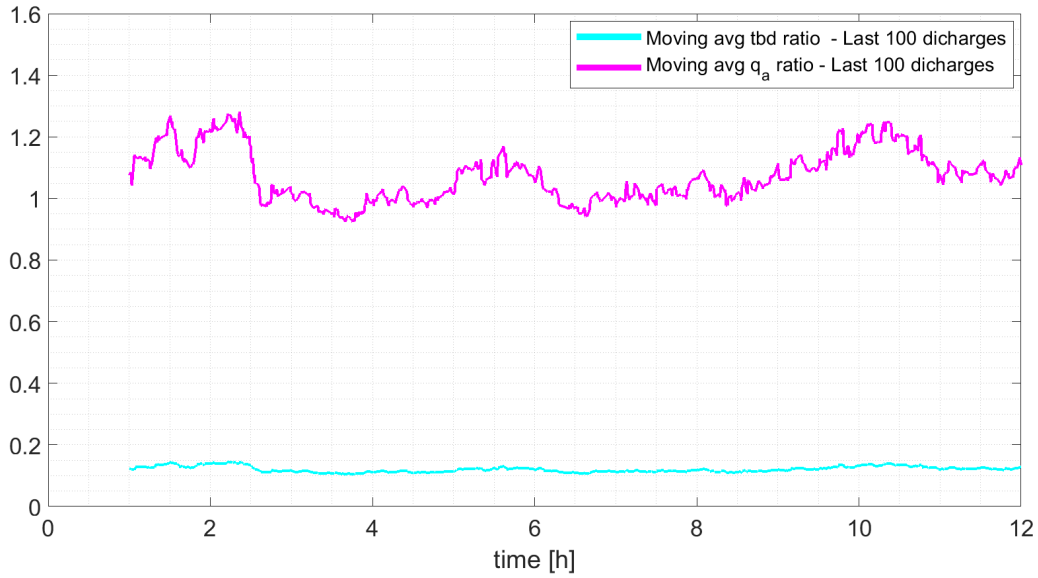

Figure 5.3: $ratio_{tbd}$ and $ratio_{q_a}$ with a moving average from the last 100 discharges for the stochastic model with 2 mm and 6 mm diameter cavities.

In order to acknowledge the general relation between both voids (2 mm and 6 mm diameter cavities), using equation eq. 5.6 it was found

$$k_{total} = 9$$

meaning the relation between this two cavities, ideally, would be of 9, following the assumptions mentioned in section 3.1. From Figure 5.4, it can be observed the k_{total} moving average for the last 100 discharges follows a fluctuating trend around the mentioned value of 9, but it is not a constant value throughout the whole simulation. This is due to the stochastic behaviour of the starting electron rate, which affects the final result.

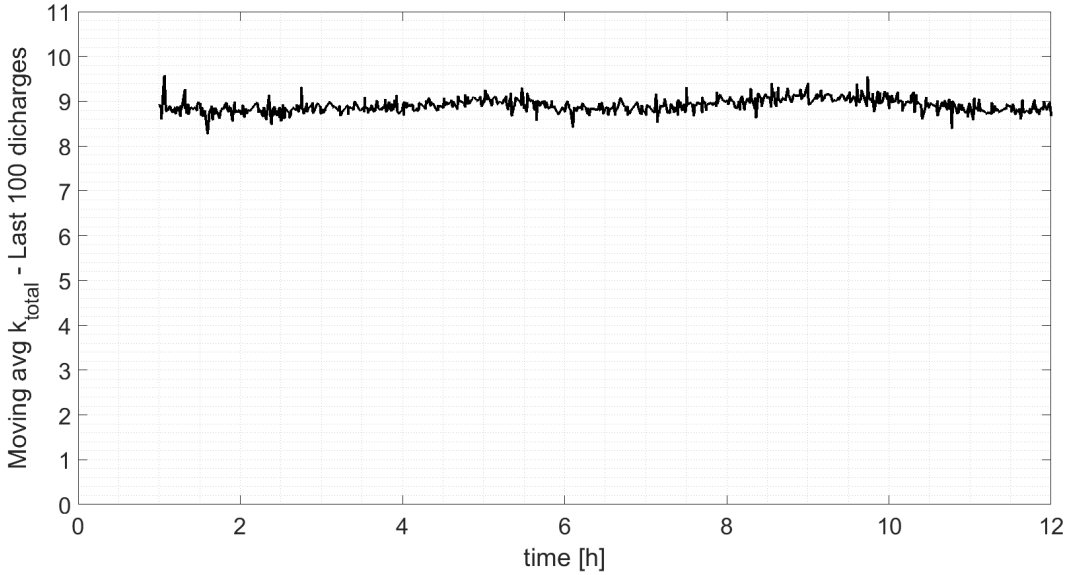

Figure 5.4: k_{total} with a moving average from the last 100 discharges for the stochastic model with 2 mm and 6 mm diameter cavities.

5.2.1 Data loss

During testing it is possible that some data cannot be recorded due to different factors, such as discharge magnitudes over the measuring device saturation limit or discharge magnitudes below the measuring threshold value of the set-up. In this section, the moving averages for the time between discharges, the discharge magnitude and k_{total} using the stochastic prediction model are going to be used to compare a case where there is no data loss and one where data is lost. It is going to be assumed that the lower discharges of the recorded data for the 6 mm cavity diameter sample is lost. The discharges that are going to be assumed lost are those with an amplitude of 25 % or lower than the calculated average.

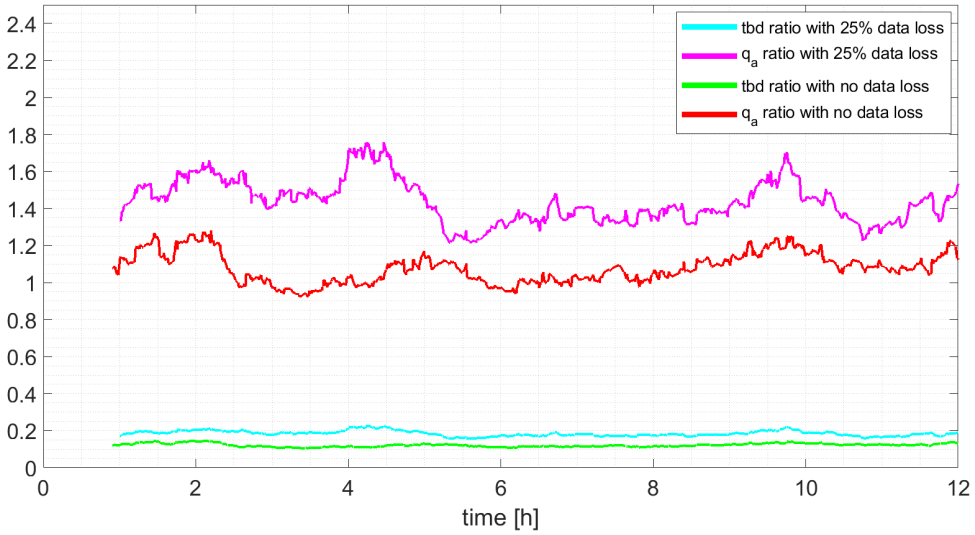

Figure 5.5: $ratio_{tbd}$ and $ratio_{q_a}$ with a moving average from the last 100 discharges for the stochastic model with 2 mm and 6 mm diameter cavities considering the events with a discharge magnitude under 25 $\%$ of the calculated average are not taken into account compared with the case where no data is lost.

Observing Figure 5.5, it can be gathered that due to this lost data factor, the time between discharges ratio and the discharge magnitude ratio increase their value, affecting both ratios. From Figure 5.6 it can be gathered the overall relation (k_{total}) decreases by one unit.

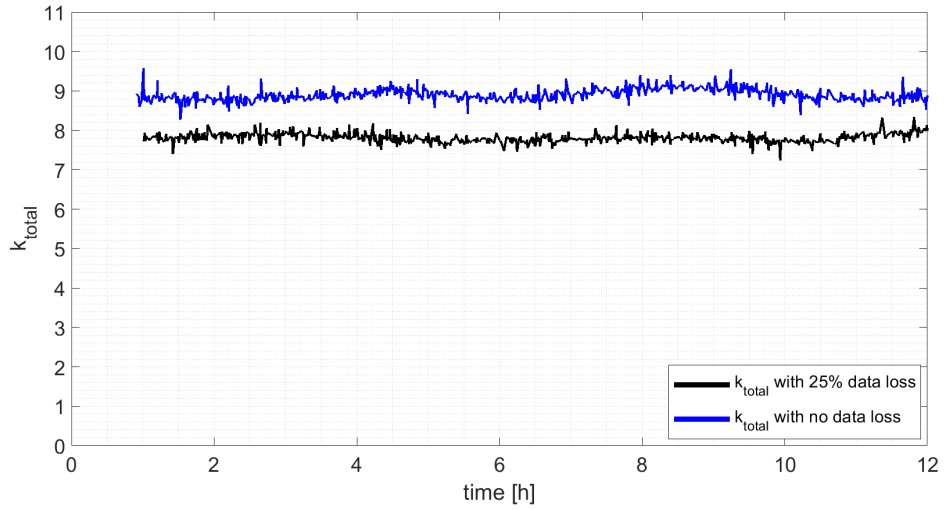

Figure 5.6: k_{total} with a moving average from the last 100 discharges for the stochastic model with 2 mm and 6 mm diameter cavities considering the events with a discharge magnitude under 25 $\%$ of the calculated average are not taken into account compared with the case where no data is lost.

Chapter 6

Experimental results

6.1 Set-up confirmation

In order for the voltage over the test object to be 10 kV DC, since there is a resistive divider in the set-up, the voltage applied for all the following tests was 12 kV DC . The ceramic capacitors ($C_s = 715\ pF$ and $C_d = 5900\ pF$) are the ones utilised for the experiments in this section.

6.1.1 Noise test at 77 °C

6.1.1.1 Test 0: $C_s = 715\ pF$ - $C_d = 5900\ pF$ with PET disk sample

To ensure the well-functioning of the final Partial Discharge measuring set-up, a noise test was performed. This test also determined the threshold chosen for the following Partial Discharge tests. For the current experiment, the threshold was adjusted manually until the value of 350 fC was decided. The duration of the test was 48 hours. It was observed that the discharges produced constant noise up to 350 fC, so the threshold for the coming tests was decided to be 400 fC.

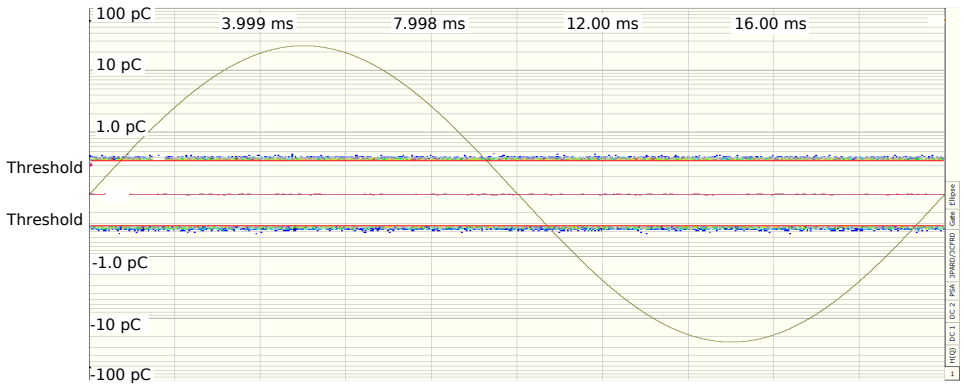

Figure 6.1: 12 kV DC test at 77 °C for $C_s = 715\ pF$ and $C_d = 5900\ pF$, disk sample and 350 fC threshold.

6.2 Partial Discharge detection

The aim of this section is to present the recorded data during the laboratory tests: the discharge magnitudes and time between discharges evolution with time. The polarity of the discharges was not considered, therefore only the absolute value of the discharge value is taken into consideration. All the tests had a duration of 48 hours.

6.2.1 Partial Discharge tests at 77 °C

6.2.1.1 Test 1: 3 x 0.075 mm PET with 2 mm Ø cavity sample

The sample for this test was glued by Olsen during his doctoral work [13] and there was no previous record on the whereabouts or tests for the sample before it was cleaned for the experiment. The threshold for this specific test was set to 450 fC. From Figure 6.2 it can be gathered that most of the discharges have a value below 10 pC.

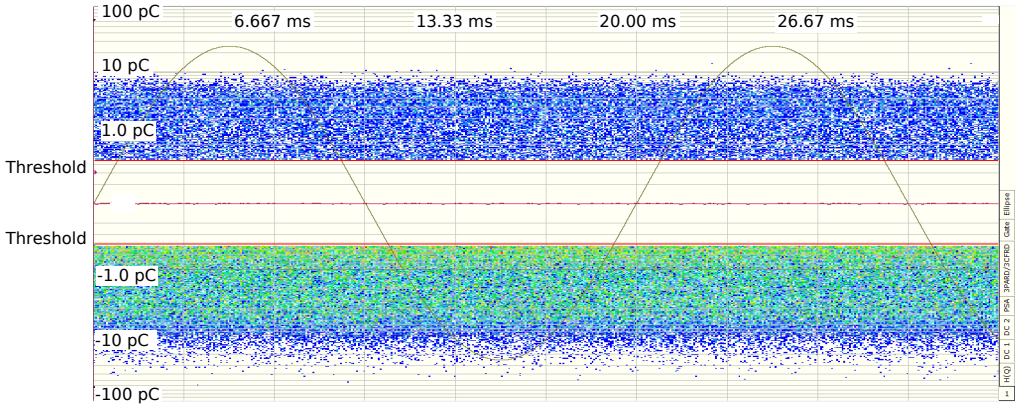

Figure 6.2: 12 kV DC test at 77 °C for a 2 mm Ø cavity sample with a 450 fC threshold.

In Figure 6.3 it is shown how the discharge magnitude and the time between discharges follow the same trend. It an also be noticed that it takes around 36 hours for the parameters to stabilize. The time between discharges (dark blue) and the discharge magnitudes (black) events are represented as dots and the moving average for the time between discharges (cyan) and the moving average for the discharge magnitudes (magenta) are represented as continuous lines. Between hour 24 and hour 28 an anomaly is recorded. This phenomenon can be due to the unknown record of the sample, since the test object could have been exposed to high electric fields, humidity or other unknown factors creating permanent defects in the sample.

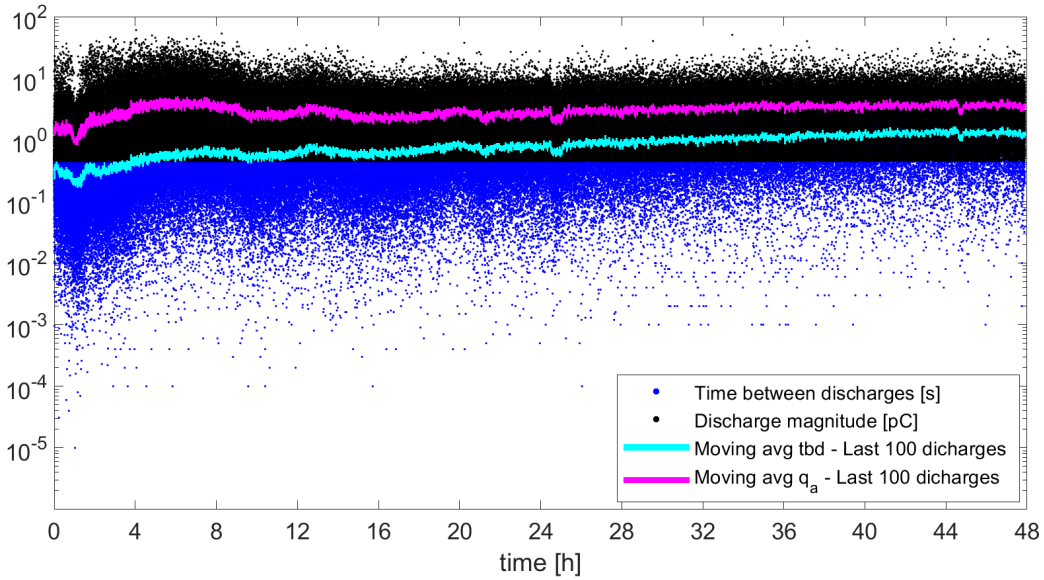

Figure 6.3: Time between discharges and discharge magnitude at 12 kV DC, 77 °C for a 2 mm Ø cavity sample.

6.2.1.2 Test 2: 3 x 0.075 mm PET with 6 mm Ø cavity virgin sample

The sample used for this test was a 6 mm diameter virgin cavity manufactured in the laboratory and kept at room temperature until the test. In Figure 6.4 it can be observed the discharge magnitudes are smaller than for the 2 mm cavities. Since there is more likely that an electron is present in the 6 mm diameter cavity (see section 2.4.1), the time lag is shorter, therefore the discharge magnitude is smaller.

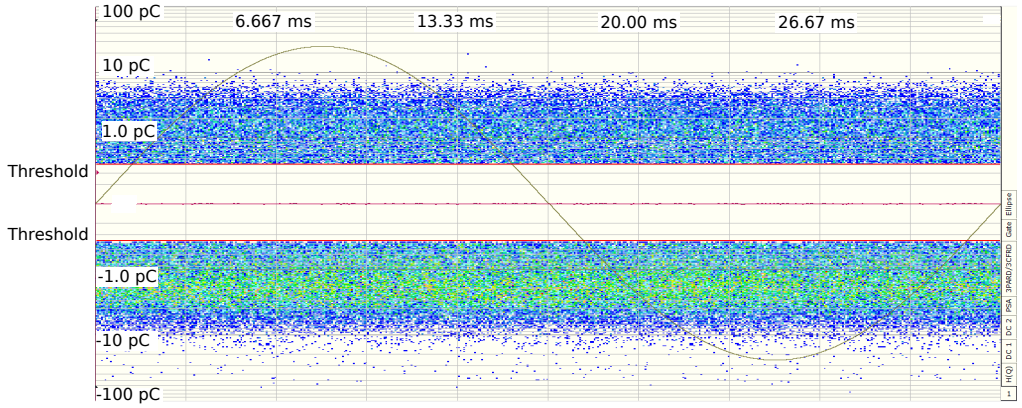

Figure 6.4: 12 kV DC test at 77 °C for a 6 mm Ø cavity virgin sample with a 400 fC threshold.

In Figure 6.5 it can be observed the moving average for the time between discharges (cyan) and the moving average for the discharge magnitudes (magenta), which are represented as continuous lines, have a steady behaviour and there are no clear anomalies throughout the testing time. However, due to the low values of the discharge magnitudes there is probably some

data loss. This affects the discharge magnitudes but it is more significant in the time between discharges. From the comparison between the trend of the discharge magnitude and the time between discharges, whereas the discharge magnitude stabilises around hour 16, the time between discharges keeps slowly increasing for the whole test.

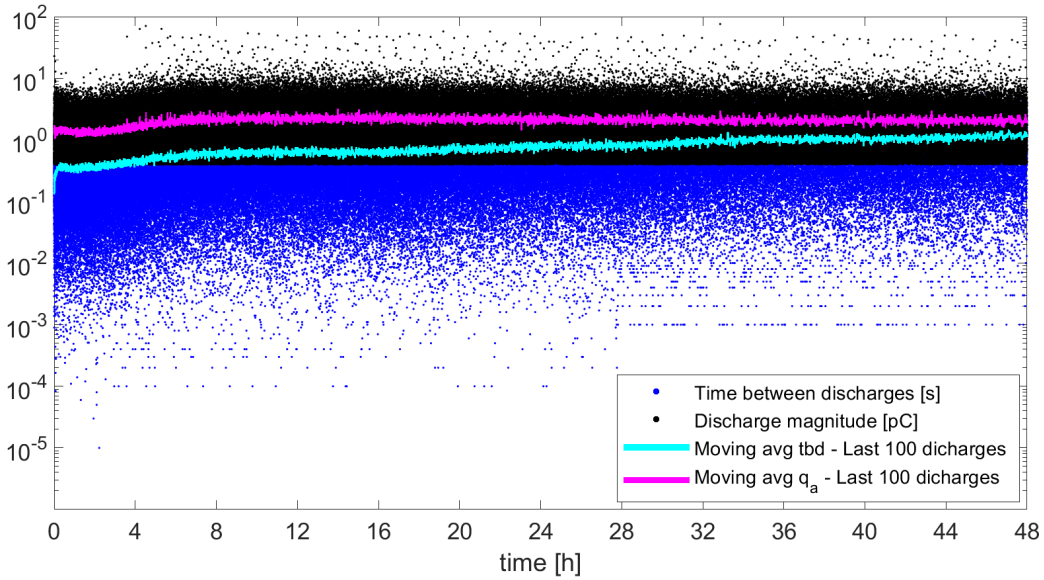

Figure 6.5: Time between discharges and discharge magnitude at 12 kV DC, 77 °C for a 6 mm Ø cavity virgin sample.

6.2.1.3 Test 3: 3 x 0.075 mm PET with 2 mm Ø cavity virgin sample

The sample used for this test is a virgin sample with a 2 mm diameter cavity. The sample was kept at room temperature until testing. From the data obtained in this experiment (see Figure 6.6) it can be observed the number of discharges seems to be inferior than test 2 and the discharges are scattered over the whole spectrum spreading up onto the recording threshold, which can result in some data loss for the higher discharge magnitudes due to saturation of the measuring device.

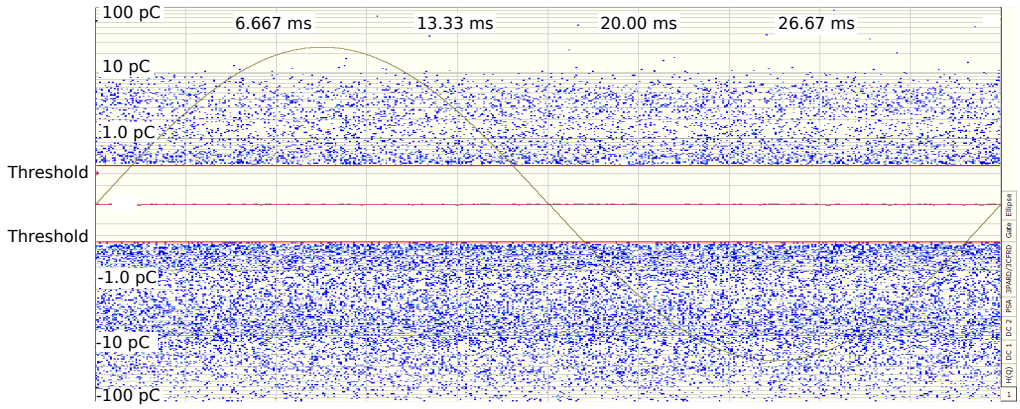

Figure 6.6: 12 kV DC test at 77 °C for a 2 mm Ø cavity virgin sample with a 400 fC threshold.

From Figure 6.7 can be gathered that the moving average for the discharge magnitude (magenta) and for the time between discharges (cyan) follow the same trend as it was expected (see section 2.6). It can also be extracted that both parameters stabilize around hour 24 and there seem to be no anomalies in the recorded data.

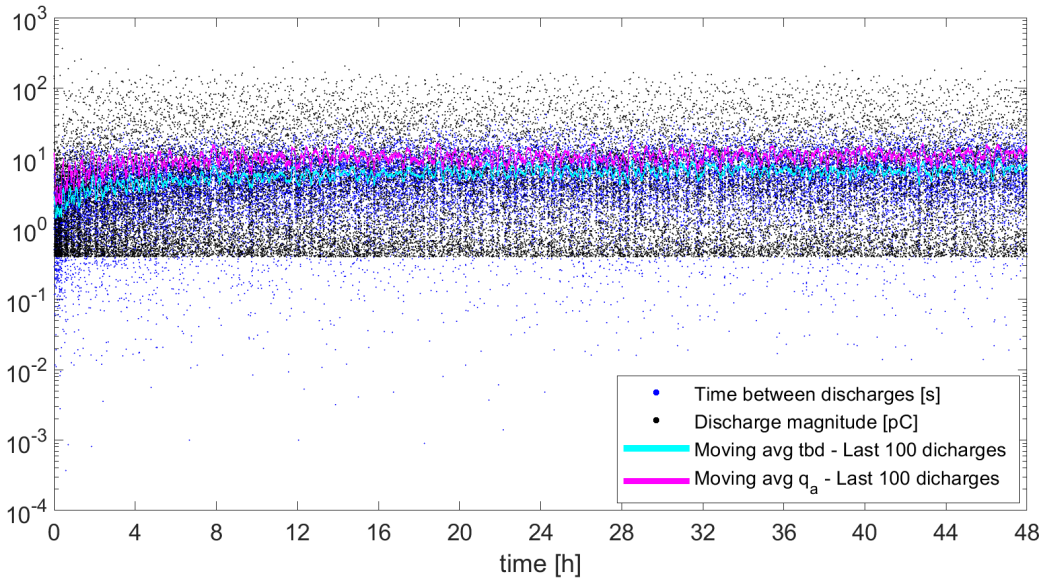

Figure 6.7: Time between discharges and discharge magnitude at 12 kV DC, 77 °C for a 2 mm Ø cavity virgin sample.

6.2.1.4 Test 4: 3 x 0.075 mm PET with 6 mm Ø cavity virgin sample

For the present experiment, a 6 mm diameter cavity virgin sample was kept at room temperature until testing. From Figure 6.8 it can be observed that most of the discharge magnitudes are below the 10 pC and there is a high density of them between the low threshold (400 fC) and the 10 pC value.

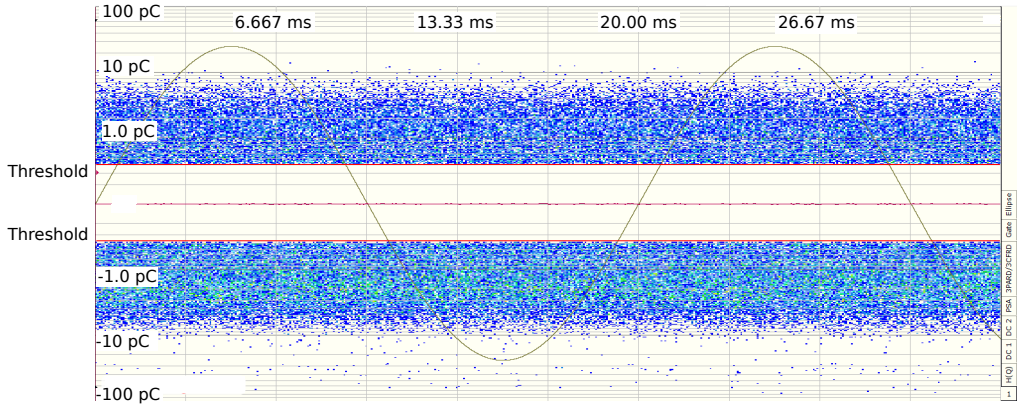

Figure 6.8: 12 kV DC test at 77 °C for a 6 mm Ø cavity virgin sample with a 400 fC threshold.

In Figure 6.9 it is possible to perceive that the moving average for the discharge magnitude (magenta) seems to reach a steady state around hour 12, whilst the moving average for the time between discharges (cyan) increases until 40 hours into the test and then it seems to stabilize. Theoretically both parameters should follow the same trend, but it is not the case for this test. A loss of data due low discharge magnitudes that cannot be recorded is a feasible explanation for that to occur.

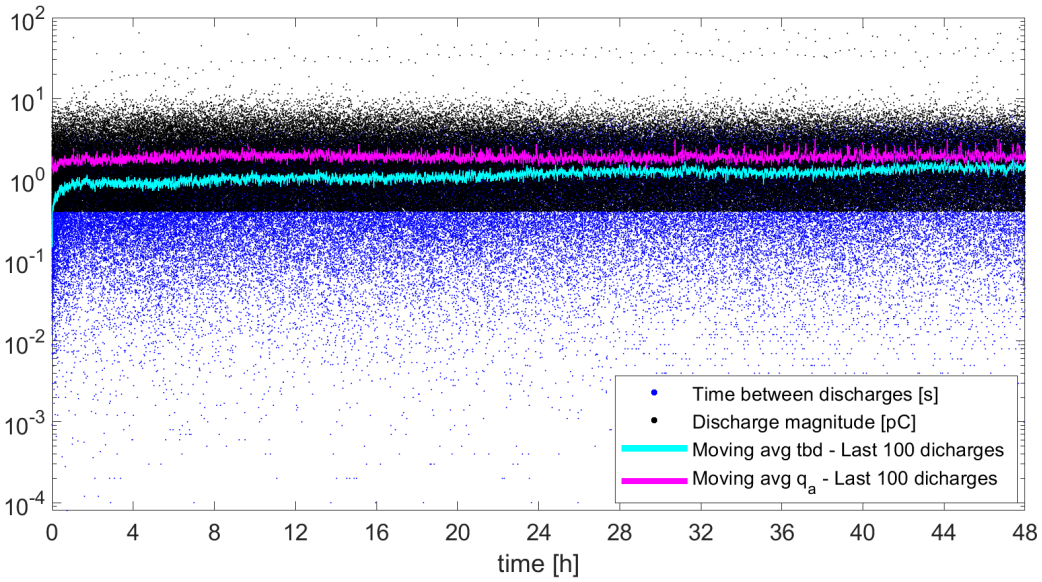

Figure 6.9: Time between discharges and discharge magnitude at 12 kV DC, 77 °C for a 6 mm Ø cavity virgin sample.

6.2.2 Partial Discharge tests at 69 °C

6.2.2.1 Test 5: 3 x 0.075 mm PET with 6 mm Ø cavity virgin sample

The sample used for this test was a 6 mm diameter virgin sample. The sample preparation process was done at room temperature and there was no temperature change applied to the sample until testing. Due to the lower testing temperature compared with the previous tests, the amount of events decreased since the conductivity is temperature dependent. When the temperature decreases, the conductivity decreases and this leads to fewer discharges.

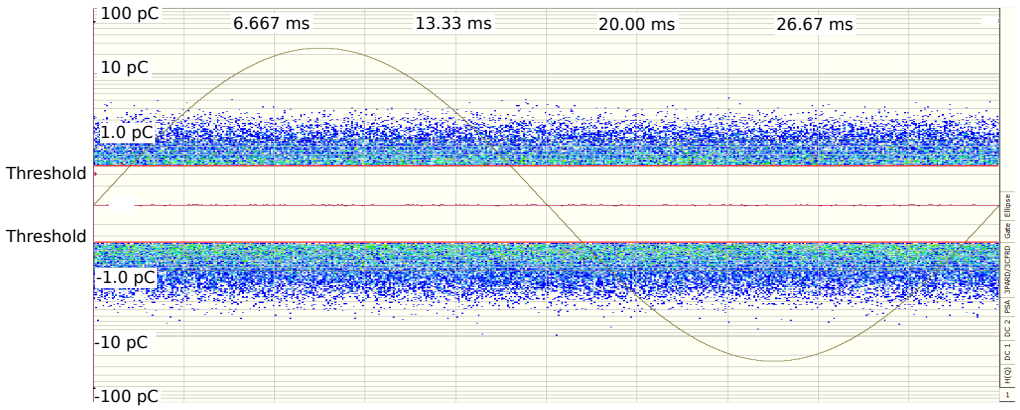

Figure 6.10: 12 kV DC test at 69 °C for a 6 mm Ø cavity virgin sample with a 400 fC threshold.

In Figure 6.11 it can be observed the discharge magnitude moving average seems to be steady throughout the whole test, whereas the time between discharges appear to stabilize around hour 32 in the test. At the beginning of the experiment, when the space charges accumulation is occurring, there is a disparity between the time between discharges and the discharge magnitude, but 32 hours into the test, this phenomenon is probably completed and then they follow the same trend.

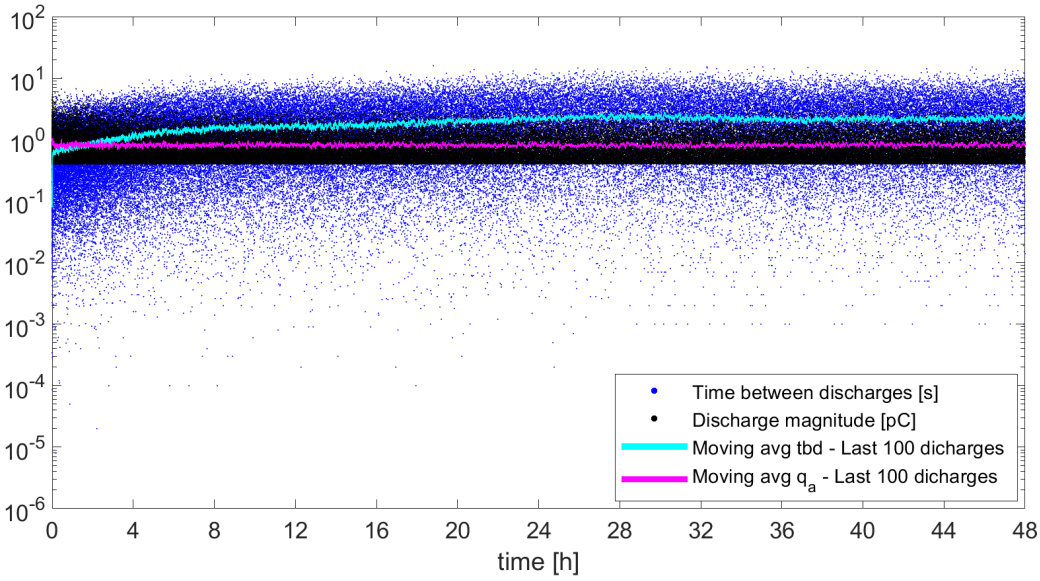

Figure 6.11: Time between discharges and discharge magnitude at 12 kV DC, 69 °C for a 6 mm Ø cavity virgin sample.

6.2.2.2 Test 6: 3 x 0.075 mm PET with 2 mm Ø cavity virgin sample

A 2 mm diameter cavity virgin sample kept at room temperature after assembly was utilised for this test. In Figure 6.12 the magnitude of discharge values is shown and it can be gathered that the amount of discharges has been reduced in comparison with the experiments held at 77 °C

since the conductivity of the PET decreases with temperature. A reduction in the number of discharges can be also due to the fact the cavity diameter is reduced, in contraposition to the 6 mm diameter cavity size for the same temperature. Several of the discharges are close to the recording threshold, hence it is likely some data has been lost during the test due to saturation of the measuring device.

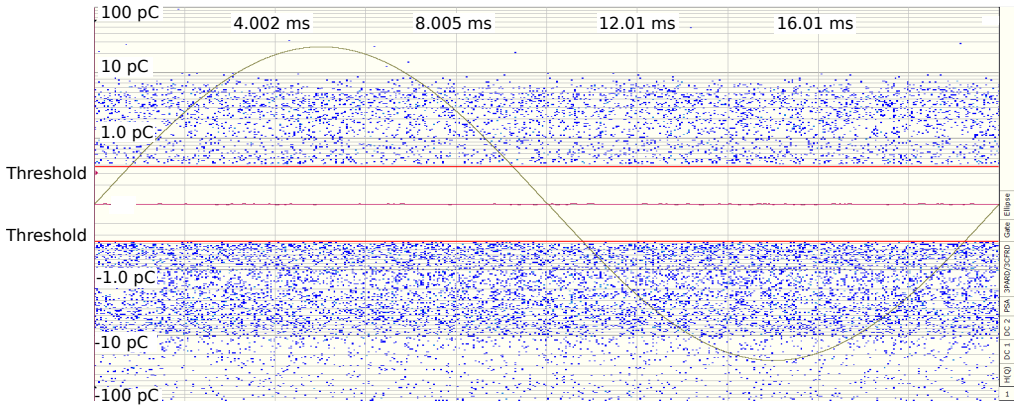

Figure 6.12: 12 kV DC test at 69 °C for a 2 mm Ø cavity virgin sample with a 400 fC threshold.

Observing Figure 6.13 it stands out there are periods, specially at the beginning of the test, where empty bands are denoting a lack of discharges. It is a singular phenomena but no explanation has been found during this work. Neglecting these events, the rest of the data seems to be following a steady trend with no apparent anomalies.

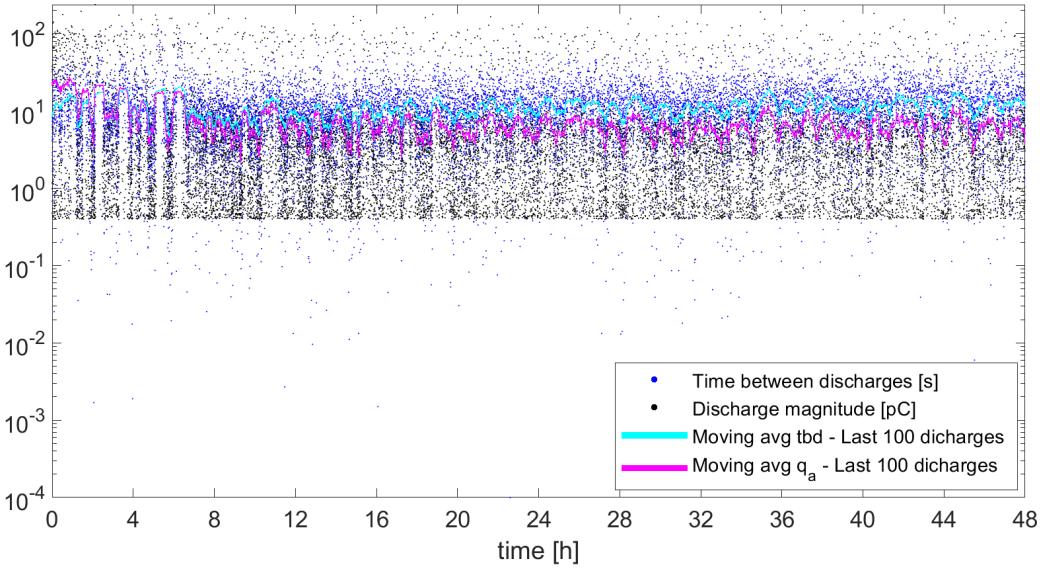

Figure 6.13: Time between discharges and discharge magnitude at 12 kV DC, 69 °C for a 2 mm Ø cavity virgin sample.

Chapter 7

Discussion

7.1 Evaluation of PET samples with the same cavity size at 77 °C

7.1.1 2 mm diameter cavity

The comparison between two samples with 2 mm diameter cavity shows a big disparity in the discharge magnitude and the time between discharges between two different test objects. It is important to denote there was no control about the test record for the sample from test 1 (see section 6.2.1.1), neither if it had been in a harsh environment nor under thermal stresses before being used for testing for the present work. The virgin sample used for test 3 (see section 6.2.1.3) was prepared in the laboratory at room temperature. In Figure 7.1 it can be observed that for both test objects, the discharge magnitude follows the time between discharges magnitude trend, which was expected. When comparing the time between discharges and the discharge magnitude of both samples, they are not coincident with each other.

Ideally, if the samples were identical, a similar behaviour would have been expected. The sample from test 1 has lower discharge magnitude and shorter time between discharges, whereas the virgin sample has higher discharge magnitudes and longer time between discharges. The lower values for the sample from test 1 can explained because it might had been subjected to humid environments, which causes the conductivity of the PET to increase, leading to shorter time between discharges and lower discharge magnitudes.

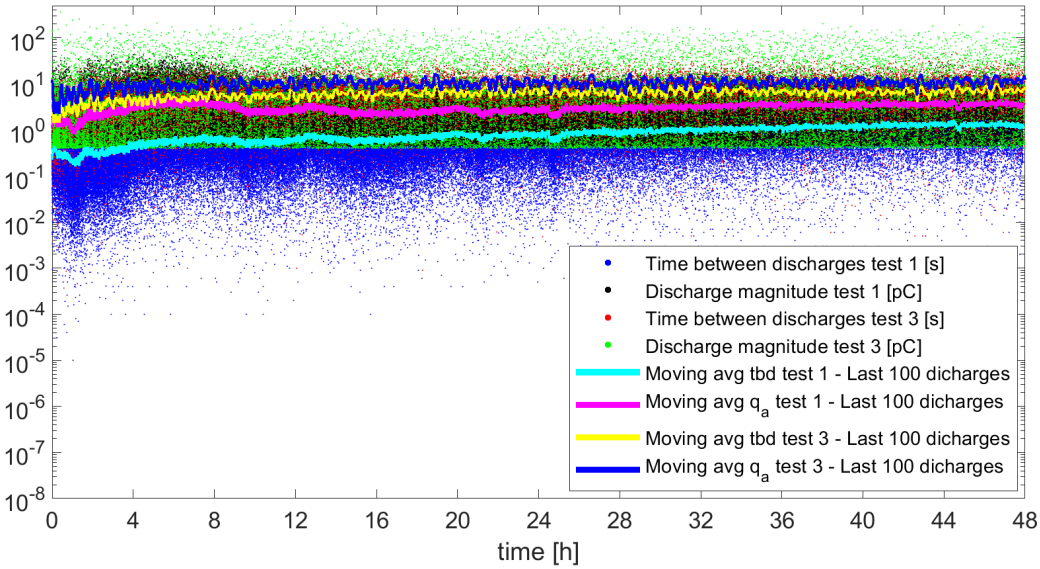

Figure 7.1: Time between discharges and discharge magnitude comparison between test 1 (2 mm Ø cavity sample) and test 3 (2 mm Ø cavity virgin sample).

7.1.2 6 mm diameter cavity

In this section two virgin samples of 6 mm cavity diameter prepared in the lab at room temperature are compared. Supposedly, if the environmental conditions when preparing both samples and the material used is the same (PET), when tested under the same conditions, the performance should be similar even if there is a stochastic behaviour due the starting electron generation rate.

From Figure 7.2, it can be gathered that the discharge magnitude moving average for both samples has a resemblant behaviour but there is more disparity for the time between discharges, where the moving averages do not follow a similar path throughout the testing time. While the discharge magnitude for both cases remains analogous, the time between discharges for test 2 (see section 6.2.1.2) is shorter than for test 4 (see section 6.2.1.4) even though the samples are supposed to be comparable. One of the possible explanations of this phenomenon can be the loss of data during testing, since some discharge magnitude values can be below the cut-off threshold and it affects the recorded measurements. Another feasible explanation for the distinct behaviours can be that the samples have not been in a controlled environment for a certain period of time before testing, thus the test objects have nonidentical physical properties. From this comparison it can be extracted that the time between discharges is influenced in a more important manner.

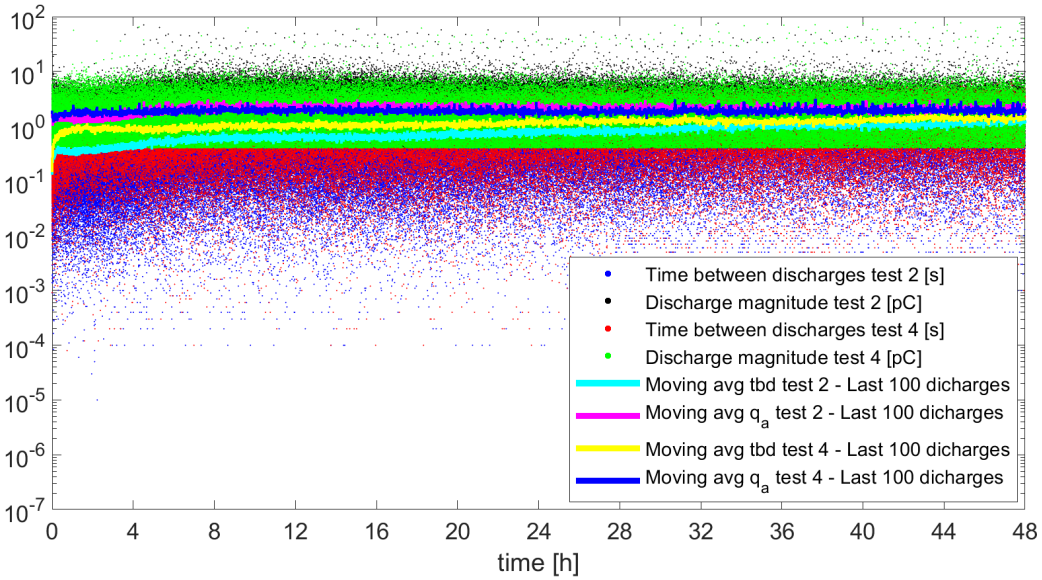

Figure 7.2: Time between discharges and discharge magnitude comparison between test 2 and test 4, both 6 mm Ø cavity virgin samples at 77 °C.

7.2 Evaluation of PET samples with the same cavity size for different temperatures

7.2.1 6 mm diameter cavity

For this section, two virgin 6 mm diameter cavity samples at 77 °C and 69 °C are compared. From Figure 7.3, the most noticeable disparity is the time between discharges variation. The sample at 77 °C has shorter time between discharges than the one at 69 °C. This was expected because the time between discharges is inversely proportional to the conductivity (see section 2.4.4), and since the temperature decreases, so does the conductivity.

A noticeable phenomenon for the present analysis is the magnitude of discharges' abnormal behaviour. Theoretically, when the conductivity decreases, the time between discharges is increased, leading to higher discharge magnitude, but for this comparison, the discharge magnitude's moving average is lower when the temperature is lower. A feasible explanation for this strange behaviour can be that for the test at 77 °C some data is lost due to discharges occurring below the noise threshold, which would increase the average value of the discharge magnitudes, and for the test at 69 °C some data might be lost due to the upper saturation limit of the measuring component, reducing the average discharge magnitude value. At the same time, for the 69 °C test, since less discharges develop, when those are not recorded, it has a more important effect because the relative amount of information lost is larger.

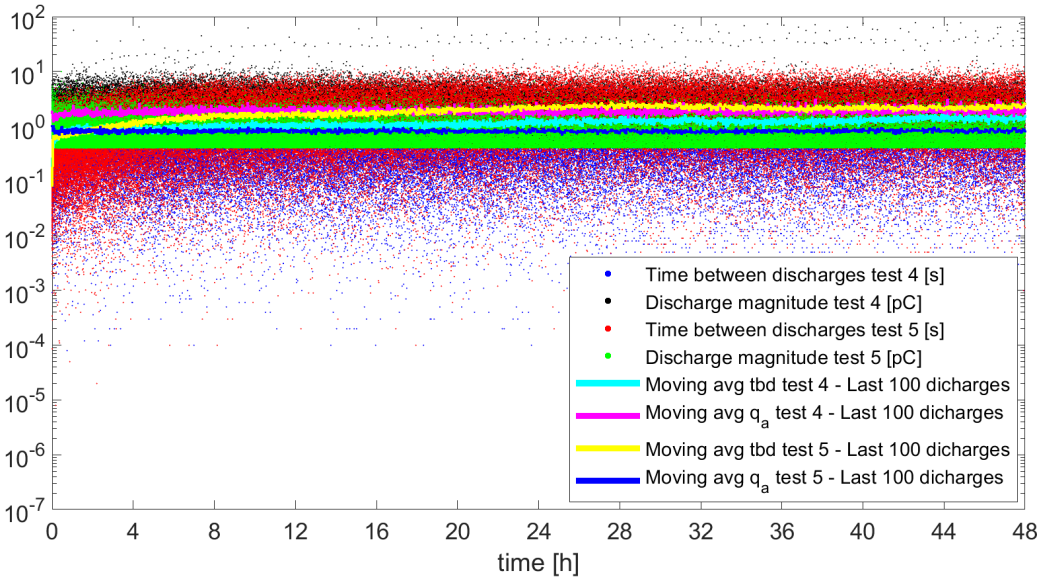

Figure 7.3: Time between discharges and discharge magnitude comparison between test 4 (6 mm Ø cavity virgin sample at 77 °C) and test 5 (6 mm Ø cavity virgin sample at 69 °C).

7.3 Evaluation of PET samples with different cavity size for various temperatures

7.3.1 2 and 6 mm diameter cavities at 77 °C

The virgin samples treated in this section had been prepared in the lab at room temperature. The difference between the samples was the diameter of the air cavity, being 2 mm for the test object used for test 3 (see section 6.2.1.3) and 6 mm for the test object used for test 2 (see section 6.2.1.2). In Figure 7.4, the time between discharges and the discharge magnitudes in regards with the duration of the test are presented. The most representative information from this comparison could be extracted after the parameters have stabilized (around hour 40). For the 6 mm diameter cavity, the moving average for the time between discharges and the discharge magnitude are lower than for the 2 mm diameter case. The shorter time between discharges was as expected because the starting electron generation rate would be higher as the area of the cavity is bigger, reducing the waiting time, which affects the time lag that at the same time is linked to the time between discharges. For the moving average of the discharge magnitude, the expectation was for them to be more similar, according to the stochastic theory (see section 2.6).

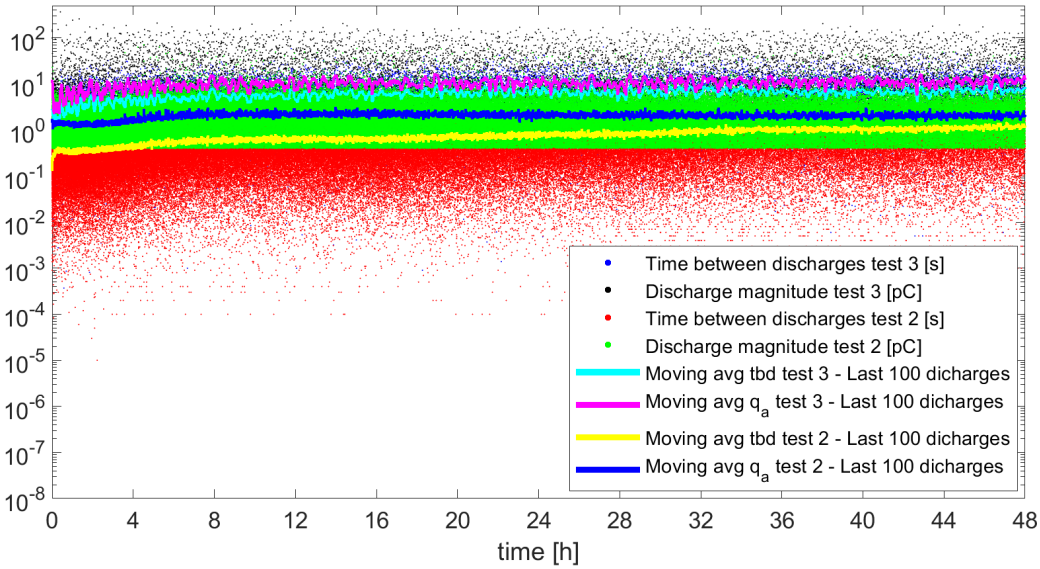

Figure 7.4: Time between discharges and discharge magnitude comparison between test 3 (2 mm Ø cavity virgin sample) and test 2 (6 mm Ø cavity virgin sample), both at 77 °C.

When observing the magnitude of discharge and the time between discharges ratios after 40 hours, both have lower values than expected. For the case of the discharge magnitude it could be already acknowledged in Figure 7.4, as both moving averages are distinct. The discharge magnitude ratio expected value was theoretically calculated to be 1, but a value close to 0.15 was found instead. For the moving average of the time between discharges, when observing Figure 7.5, the plotted value for the comparison was found to be on the whereabouts of 0.025 instead of the $\frac{1}{9}$ expected from the stochastic theory. It is impossible to extract conclusive results from a small sample population, but the difference between the theoretical values and the experimental results could might be explained due to the stochastic nature of each discharge combined with the different physical properties for each sample and the possible data loss during the measurements.

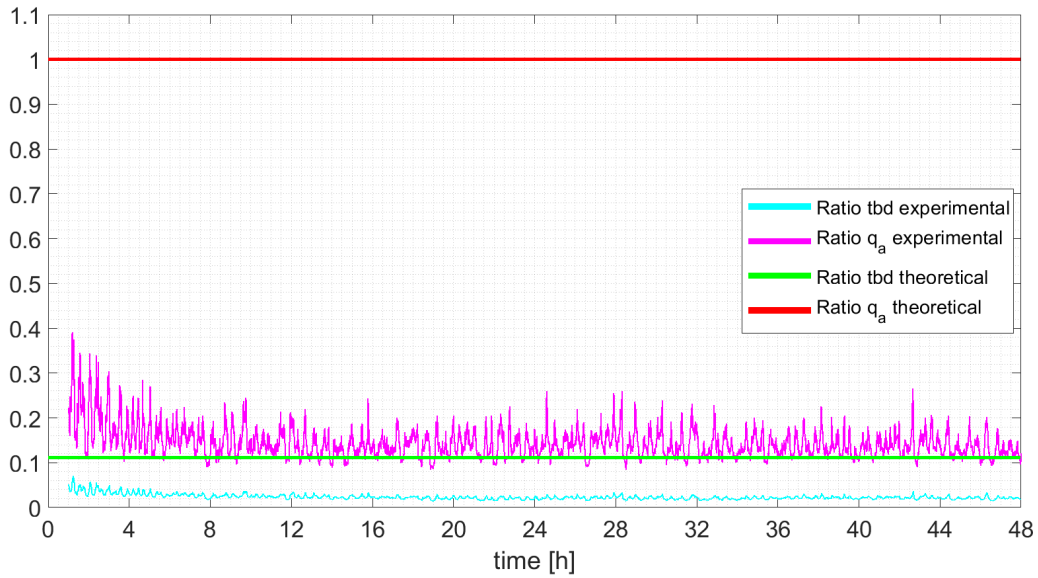

Figure 7.5: $ratio_{tbd}$ and $ratio_{q_a}$ with a moving average from the last 100 discharges found experimentally 77 °C compared with the stochastic theoretical values.

In order to take into consideration the four main parameters used to analyse the data, k_{total} is plotted with respect of the time, to show the overall trend. The highest interest lies from hour 40 of the test, where the parameters are stabilized. The k_{total} expected was of a value of 9 but the one found experimentally had a value around 6. This deviation from the expected value has been studied in section 5.2.1, where it is tested through the stochastic model, which repercussion can the coefficients suffer if some data is lost (for this specific case, in the 6 mm test). This phenomenon would explain why a lower k_{total} was found instead of the expected theoretical value along with the other possible hypothesis mentioned above in the section.

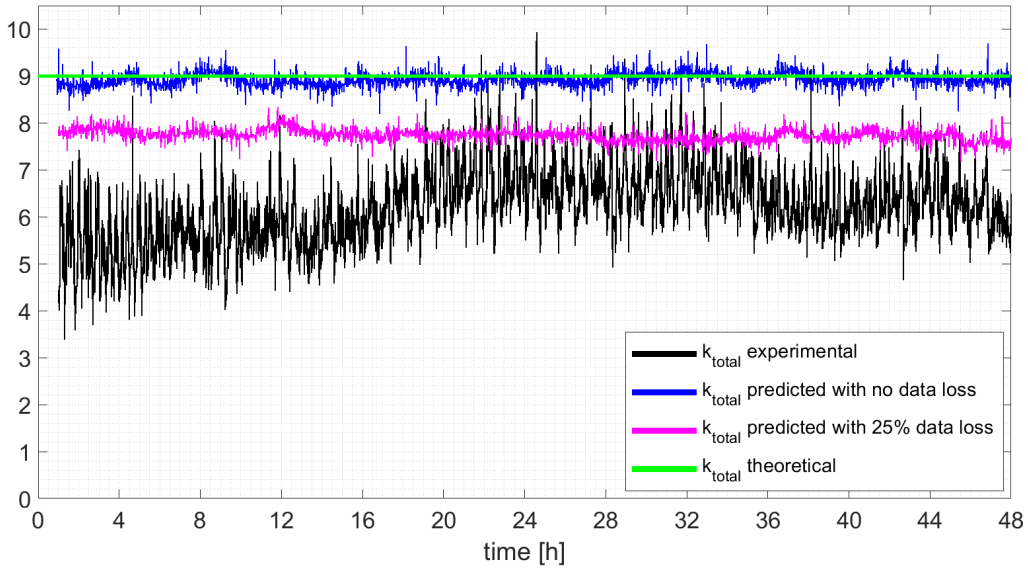

Figure 7.6: k_{total} found experimentally at 77 °C compared with the predicted value from the stochastic model with and without data loss and the stochastic theoretical value.

7.3.2 2 and 6 mm diameter cavities at 69 °C

In this section, a 2 mm diameter cavity virgin sample and a 6 mm cavity virgin sample at 69 °C are evaluated. Observing Figure 7.7, an abnormal behaviour for the 2 mm diameter cavity sample is shown during the first hours of the test, thus the analysis of the data was of interest after 35 hours, when both samples seem to be more stable. No feasible explanation was found for the anomalous behaviour for the 2 mm diameter cavity virgin sample.

The information that can be extracted from Figure 7.7 was the longer time between discharges for the 2 mm diameter cavity sample, which was expected from the theory (see section 2.6), since the starting electron generation rate (see section 2.6.1) is smaller for the 2 mm diameter cavity and this implies the time between discharges increases. In terms of the discharge magnitude, according to the theory, the values were expected to be similar for both cavities, but during the analysis of the recorded data, a different result was observed. A feasible explanation for this phenomenon can be the data loss limitation mentioned in previous sections.

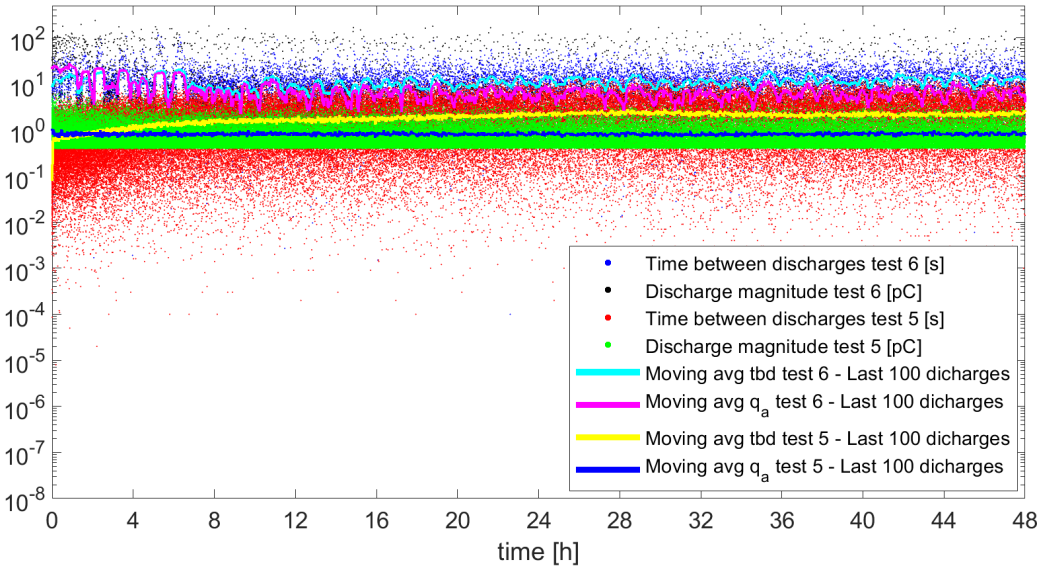

Figure 7.7: Time between discharges and discharge magnitude comparison between test 6 (2 mm Ø cavity virgin sample) and test 5 (6 mm Ø cavity virgin sample), both at 69 °C.

The time between discharges and the discharge magnitude ratios found analytically have both lower values than expected from the stochastic theory. From Figure 7.8 it can be gathered the correlation between the discharge magnitude ratio stabilises at approximately 0.2 instead of the expected theoretical value, which was found to be of 1. For the time between discharges ratio, the theoretical value was calculated to be $\frac{1}{9}$ but it was empirically observed to stabilize round about 0.01. One of the possible explanations for this great difference between the expected and the empirical value can be the high discharge magnitude difference between both tests objects and the possible loss of data for each performed test.

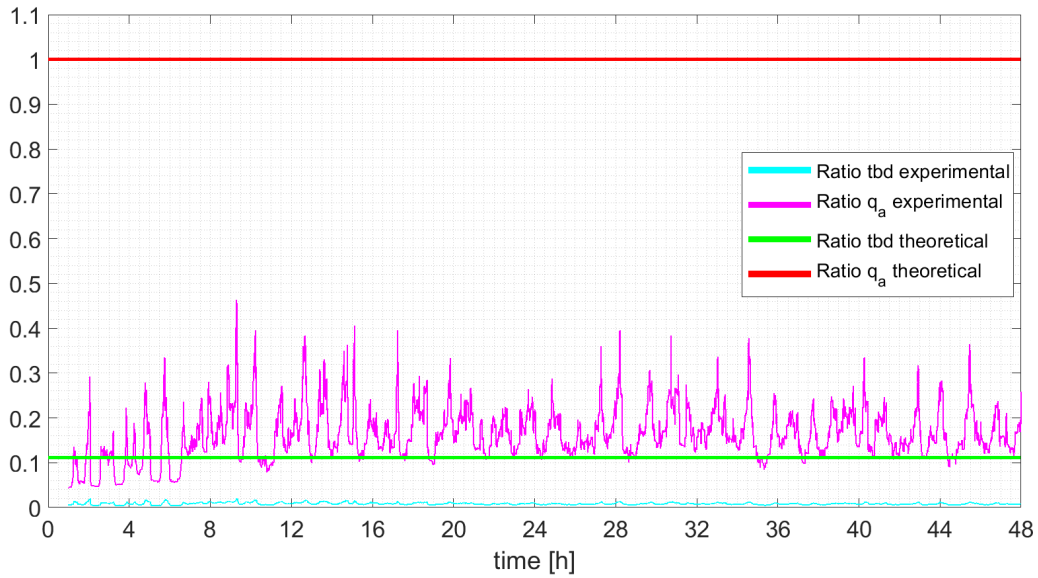

Figure 7.8: $ratio_{tbd}$ and $ratio_{q_a}$ with a moving average from the last 100 discharges found experimentally 69 °C compared with the stochastic theoretical values.

The relation between the 2 mm and the 6 mm diameter cavity at 69 °C is summarized employing k_{total}. In Figure 7.9, the value of the experimental k_{total} is shown. When it stabilizes around hour 35, the approximate value of the parameter is 20. The theoretical value for k_{total} was found to be of 9 and when the stochastic theoretical value is juxtaposed with the stochastic prediction model, the predicted moving average displays a trend around the value of 9 as well. One possible explanation for this big variation in the lab tests can be the nature of the discharges. Since the temperature decreases, the likelihood of streamers occurring increases [7]. When a streamer discharge occurs, the cavity is discharged and, unlike Townsend discharges, the cavity is ready to discharge again [7]. Streamer discharges have a different nature than Townsend discharges (see section 2.4) and the possible repercussions of this types of discharges have not been covered in this thesis. Another possibility is that due to the size of the cavity, the discharges do no occur over the whole cavity, only in some parts of the surface, also leading to inconclusive results.

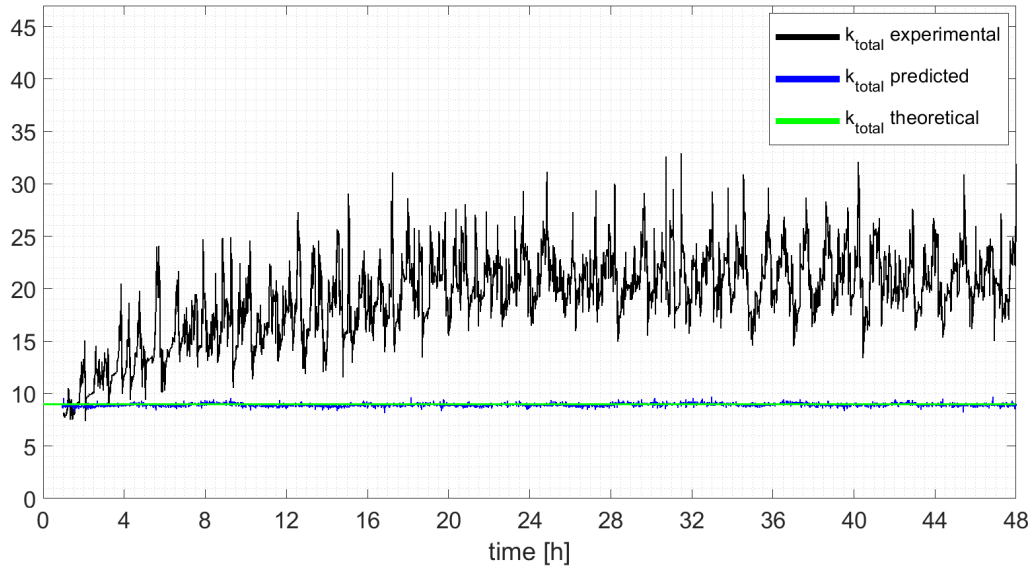

Figure 7.9: k_{total} found experimentally at 69 °C compared with the predicted value from the stochastic model with and without data loss and the stochastic theoretical value.

Chapter 8

Conclusion

The main aim of this master thesis was to improve the sensitivity of the HVDC and high frequency AC voltage Partial Discharge measuring set-up [2], ensure the well-functioning of the new set-up, perform DC tests to detect Partial Discharges in PET samples with different cavity sizes and generate High Voltage DC models for relative comparison with the laboratory tests and theory. It is important to mention the samples' thickness for all the Partial Discharge measurements had been the same. The only difference on the samples construction had been the cavity diameter, thus reducing the amount of variables affecting the analysis of the tests.

The conclusions extracted from the results and the discussion in this thesis are presented as follows:

- A successful set-up for measuring Partial Discharges under DC has been achieved and Partial Discharge measurements for High Voltage DC have been performed with the improved set-up.
- High Voltage DC Partial Discharge prediction models have been successfully generated in Matlab for a relative comparison of different cavity sizes following the deterministic and the stochastic theories.
- A correlation between the cavity diameter and the time between discharges has found to be present during the laboratory tests, with a similar behaviour as predicted in the models and presented in the theory. When the cavity diameter is smaller, the starting electron rate is smaller, therefore the time between discharges increases. For the bigger diameter a similar behaviour has been observed, since a bigger cavity has a higher starting electron generation rate, thus the time between discharges decreases. The High Voltage DC deterministic model is unsuccessful at describing the behaviour, however the High Voltage DC stochastic model provides a proper relative prediction, with a similar behaviour but distinct value.

- The discharge magnitude has a similar behaviour as the time between discharges regarding the cavity diameter. For a decreasing cavity diameter, the discharge magnitude increases in view of the fact the starting electron generation rate decreases. The High Voltage DC stochastic model and the experimental results are in consonance. However, the experimental results differ in the magnitude of this correlation.
- The temperature affects the time between discharges and the discharge magnitude. A reduction in temperature reduces the conductivity of the PET, thus increasing the time between discharges and the discharge magnitude. A prudent approach has to be taken for this conclusion, considering when the different temperature tests were performed, the nature of the cavities was intrinsically different and the limitations from the measuring devices were also a factor.
- From the two High Voltage DC models created for this thesis, the stochastic model has provided a more accurate relative prediction of the analysed parameters to the laboratory results than the deterministic model, even though it is not possible to have an absolute comparison between the models and the empirical tests.
- The nature of the samples used for measuring DC Partial Discharges were different for each test object, which hindered the reproducibility of the experiments.

For the present work, discrepancies between the relative data extracted from the stochastic model and from experimentation has been found. A brief mention of the possible sources that are thought to be the principal distinguishing factors are: the phenomena occurring in the lab are much more complex than the stochastic prediction model, the data loss during the experiments and the non-reproducibility of the environmental conditions for the test samples.

The conducted work presented some limitations. The measuring equipment for Partial Discharges can be a constraint since it becomes more challenging to record the PD events for DC voltage because of the significantly smaller discharge magnitude than for AC voltage. Due to the limited time for this thesis, a reduced amount of tests were performed, therefore the results are not statistically significant and could be subjected to variation. A larger test population for each experiment would, thus provide more consistent empirical data to contrast. The behaviour of the events could have been affected by the difference between the chosen cavity diameters size, thus voids with diameters within those performed during this present work are thought to be of great interest.

Chapter 9

Further Work

The present work is a portion of the vast amount of possibilities the Partial Discharge field of knowledge can provide. The work for this thesis could be expanded in further projects:

- Increase the population for each test for a more reliable and comparable set of data.
- Standardisation of the samples preparation to favour the reproducibility of the experiments. A suggestion towards the goal could be to store the samples in a controlled environment for a certain amount of time, attempting to replicate the same intrinsic conditions for all the test objects.
- Permittivity and conductivity measurements at different temperatures for the material utilised for the Partial Discharge experiments is of high interest since acquiring knowledge of the material properties and how do they evolve can help understand the overall behaviour of the samples.
- Maintaining the same cavity geometry, it can be of interest to change the location of the cavity (in the top and bottom sheet) and the thickness to observe which behaviour changes can betide.
- Different cavity geometries to behold how it can affect the Partial Discharge demeanour.
- Utilisation of other materials used for HVDC insulation (e.g. XLPE) for sample construction with various thickness.
- Implementation of a second MPD 600 to provide a wider range for the measuring set-up and/or alternatively the usage of the universal partial discharge measurement and analysis system MPD 800.
- Expansion of the High Voltage DC models introducing a variable $\frac{dV}{dt}$, conductivity with temperature dependency, etc. and fine tuning of the stochastic model in order to achieve an absolute comparable model with the empirical data.

- The realisation of the above mentioned work aimed to encompass the HVDC with high frequency AC voltage is highly encouraged.

References

[1] S. D. Wright, A. L. Rogers, J. F. Manwell, and A. Ellis, "Transmission options for offshore wind farms in the united states," *Proceedings of the American Wind Energy Association Annual Conference*, pp. 1–12, 2002.

[2] P. Olsen, I. Velo, and F. Mauseth, "Experimental challenges when measuring partial discharges under combined DC and high frequency AC voltage," *Proceedings of the Nordic Insulation Symposium*, Sept. 2017.

[3] J. Martí Cascalló, "Design and evaluation of a test set-up for partial discharge tests under combined DC and AC voltage," Norwegian University of Science and Technology, Department of Electrical Power Engeneering, Project report in TET5500, Dec. 2019.

[4] E. Ildstad, *TET4160 Insulating Materials for High Voltage Applications*. NTNU Department of Electric Power Engineering, 2008.

[5] *IEC 60270. High-voltage test techniques - Partial discharge measurements*. 3.1.IEC, 2015.

[6] J. Pihera, R. Haller, and P. Mráz, "Partial discharges evaluation at DC voltage," *Proceedings of the 2014 15th International Scientific Conference on Electric Power Engineering*, 2014.

[7] U. Fromm, "Partial discharge and breakdown testing at high DC voltage," *PhD Monograph, Delft University of Technology*, 1995.

[8] K. C. Kao, *Dielectric Phenomena in Solids*. Academic Press, 2004.

[9] E. Kuffel, W. S. Zaengl, and J. Kuffel, *High Voltage Engineering: Fundamentals*. Butterworth-Heinemann, 2000.

[10] R. Bartnikas and E. J. McMahon, *Engineering Dielectrics. Volume I. Corona measurement and interpretation*. American Society for Testing and Materials, 1979.

[11] P. Morshuis and L. Niemeyer, "Measurement and simulation of discharge induced age-

ing processes in voids," *IEEE Annual Report - Conference on Electrical Insulation and Dielectric Phenomena*, October 1996.

[12] L. Niemeyer, "A generalized approach to partial discharge modeling," *IEEE Transactions on Dielectrics and Electrical Insulation*, vol. 2, no. 4, pp. 510–528, August 1995.

[13] P. K. Olsen, "Internal partial discharges at high DC voltage and the effect of superimposed AC voltage," Ph.D. dissertation, Norwegian University of Science and Technology, Publication pending.

[14] J. C. Devins, "The physics of partial discharges in solid dielectrics," *IEEE Transactions on Electrical Insulation*, vol. EI-19, no. 4, pp. 475–495, October 1984.

[15] L. A. Dissado and J. C. Fothergill, *Electrical Degradation and Breakdown in Polymers*. IET, 2008.

Appendix A

Appendices

A.1 High Voltage DC Partial Discharges stochastic prediction model Matlab code

```
%%
clear
close all
clc


format long
%%High Voltage DC Partial Discharges stochastic prediction model

%General considerations

%%Permittivity PET
epsilon_rel=3.1; %PET
epsilon_0=8.8541878176e-12;

%%Conductivity [S/m] and resistivity [Ohm/m] PET
cond=1e-15;
resi=1/cond;

%%Permittivity and conductiviy [S/m] of air
cond_air=5e-50;  %Assuming the conductivity in air is almost zero
                 %so all the votlage drop occurs in the cavity
resi_air=1/cond_air;
epsilon_rel_air=1;
```

```
25
26 %Heigh of the sample (H) and height of the cavity (h) in [m]
27 H=250e-6;
28 h=75e-6;
29
30
31 %%Diameter and Radius of the cavity in the sample in [m]
32 D_1=0.002;
33
34 R_1=D_1/2;
35
36 D_3=0.006;
37 R_3=D_3/2;
38
39
40 %%Area of the cavity [m^2]
41 A_1=pi*R_1^2;
42 A_3=pi*R_3^2;
43
44 %%Calculating C_b
45 C_b_1=epsilon_rel*epsilon_0*(A_1/(H-h));
46 C_b_3=epsilon_rel*epsilon_0*(A_3/(H-h));
47
48 %Calculating C_c
49 C_c_1=epsilon_rel_air*epsilon_0*(A_1/(h));
50 C_c_3=epsilon_rel_air*epsilon_0*(A_3/(h));
51
52 %Calculating R_c
53 R_c_1=resi_air*((h)/A_1);
54 R_c_3=resi_air*((h)/A_3);
55
56 %Calculating R_b
57 R_b_1=resi*((H-h)/A_1);
58 R_b_3=resi*((H-h)/A_3);
59
60 %% Defining start electric generation rate per area
61
62 %Start electron generation rate Nel
63
64 tau_el = 5; % mean statistical waiting time for start electron
65
```

```
Nel=0.2;

% Nel,A [electron*s^-1*m^-2]. Start electron generation rate per area
Nel_A=Nel/(pi*0.001^2);

%Nel_cavities [electron*s^-1]
Nel_1=Nel_A*A_1;
Nel_3=Nel_A*A_3;

%%Average waiting time for startig electron
Tau_s_1=1/Nel_1;
Tau_s_3=1/Nel_3;


%%
%%The time constant

tau_1=((R_b_1*R_c_1)*(C_b_1+C_c_1))/(R_b_1+R_c_1);
tau_3=((R_b_3*R_c_3)*(C_b_3+C_c_3))/(R_b_3+R_c_3);



%%
%%V_con (Voltage across the void)

V_0=10000; %V test voltage

V_con_1=V_0*(R_c_1/(R_b_1+R_c_1));
V_con_3=V_0*(R_c_3/(R_b_1+R_c_3));

%%V_pasch
h_mm=h*1000;
p=1*1.01325;

V_min=(2420*p*h_mm+2080*sqrt(p*h_mm));

%%dV/dt
V_r=V_min; %For Townsend discharges

dV_dt_1=(V_con_1-V_r)/tau_1;
dV_dt_3=(V_con_3-V_r)/tau_3;
```

```
107
108
109
110 %%
111 %%Generating the randomised parameters
112 store_t_L_1(1)=0;
113 store_t_L_3(1)=0;
114 index=1;
115
116
117 for count = 1:10000
118
119  index=index+1;
120
121 %Commulative density function random number generator
122 cdf=rand;
123
124     %Time lag (t_L)
125     t_L_1=-((log(1-cdf))/Nel_1);
126     t_L_3=-((log(1-cdf))/Nel_3);
127
128 prop_fac=9;
129
130         %t_R/t_L=(prop_fac-1)
131         t_R_1=t_L_1*(prop_fac-1);
132         t_R_3=t_L_3*(prop_fac-1);
133
134 %Discharge magnitude
135 q_a_1=C_b_1*prop_fac*dV_dt_1*t_L_1;
136 q_a_3=C_b_3*prop_fac*dV_dt_3*t_L_3;
137
138 %Storing the variables
139
140 store_t_L_1(index)=t_L_1;
141 store_q_a_1(index)=q_a_1;
142 store_t_L_3(index)=t_L_3;
143 store_q_a_3(index)=q_a_3;
144 store_index(index)=index;
145
146 store_t_R_1(index)=t_R_1;
147 store_t_R_3(index)=t_R_3;
```

```
148
149
150 end
151
152 %%
153 %%Vector treatment
154 length_vec=length(store_t_L_1);
155
156 store_t_L_1;
157 store_q_a_1;
158 store_t_L_3;
159 store_q_a_3;
160
161 store_t_R_1;
162 store_t_R_3;
163
164
165 s_t_L_1=store_t_L_1(:,2:length_vec);
166 s_q_a_1=store_q_a_1(:,2:length_vec);
167 s_t_L_3=store_t_L_3(:,2:length_vec);
168 s_q_a_3=store_q_a_3(:,2:length_vec);
169
170 s_t_R_1=store_t_R_1(:,2:length_vec);
171 s_t_R_3=store_t_R_3(:,2:length_vec);
172
173
174
175 %%Delta_V_c (total voltage drop in the cavity)
176 Delta_V_c_1=prop_fac*dV_dt_1*s_t_L_1;
177 Delta_V_c_3=prop_fac*dV_dt_3*s_t_L_3;
178
179 %%
180 %%Average value of the total voltage drop in the cavity
181 avg_Delta_V_c_1=mean(Delta_V_c_1);  %This is the Delta_V_c value
182                                     %used for the deterministic model
183 avg_Delta_V_c_3=mean(Delta_V_c_3);
184
185
186
187 %%
188 % Time between discharges
```

```
189
190 for i=1:(length_vec-1)
191
192     t_prev_disch_1=store_t_R_1(i)+s_t_L_1(i);
193     t_prev_disch_3=store_t_R_3(i)+s_t_L_3(i);
194
195
196
197     store_t_prev_disch_1(i)=t_prev_disch_1;
198     store_t_prev_disch_3(i)=t_prev_disch_3;
199 end
200
201 %Vector with time between discharges
202 store_t_prev_disch_1;
203 store_t_prev_disch_3;
204
205 %Vector treatment
206 length_vec_tbd=length(store_t_prev_disch_1);
207
208 s_t_prev_disch_1=store_t_prev_disch_1(:,2:length_vec_tbd);
209 s_t_prev_disch_3=store_t_prev_disch_3(:,2:length_vec_tbd);
210
211
212 s_t_prev_disch_1;
213 s_t_prev_disch_3;
214
215
216 %%
217 %%Changing units of the stored values.
218 %t_L from [s] to [days] and from [C] to [pC]
219
220 s_t_L_1_days=s_t_L_1/(60*60*24);
221
222 s_t_L_3_days=s_t_L_3/(60*60*24);
223
224
225 s_q_a_1_pico=s_q_a_1*1e12;
226
227 s_q_a_3_pico=s_q_a_3*1e12;
228
229 %%q_a needs to be adjusted when comparing with tbd
```

```
s_q_a_1_pico_tbd=s_q_a_1_pico(:,2:length_vec_tbd);
s_q_a_3_pico_tbd=s_q_a_3_pico(:,2:length_vec_tbd);



%%
%Creating a time vector to simulate the labratory experiments

num=length_vec-1;
num_1=length_vec-2;
num_2=length_vec-3;

a_1=s_t_prev_disch_1;
a_3=s_t_prev_disch_3;
pp=1;

for j=2:num

    b_1=a_1(pp);
    b_3=a_3(pp);


    s_b_1(j)=b_1;
    s_b_3(j)=b_3;

    pp=pp+1;
end

s_b_1;
s_b_3;

vv=1;
bb=0;
for g=2:num

    if g<3
    c_1=s_b_1(1)+s_b_1(2);
    c_3=s_b_3(1)+s_b_3(2);

    s_c_1(vv)=c_1;
    s_c_3(vv)=c_3;
```

```
271
272     else
273
274      s_c_1(vv)=s_c_1(bb)+s_b_1(g);
275      s_c_3(vv)=s_c_3(bb)+s_b_3(g);
276
277
278     end
279     vv=vv+1;
280     bb=bb+1;
281 end
282
283 %%s_c is the time for the discharges discharges
284 %organized chornologically
285
286 s_c_1;
287 s_c_3;
288
289
290 %Vector organisation and treatment
291
292 s_q_a_1_pico_tbd;
293 s_c_1;
294 s_c_1_h=s_c_1/(60*60);
295
296 s_q_a_3_pico_tbd;
297 s_c_3_h=s_c_3/(60*60);
298
299
300 %%
301 %%Moving average
302
303 C_1=s_q_a_1_pico_tbd;
304 tbd_1=s_t_prev_disch_1;
305 t_1=s_c_1_h;
306
307 C_3=s_q_a_3_pico_tbd;
308 tbd_3=s_t_prev_disch_3;
309 t_3=s_c_3_h;
310
311 M_C_1 = movmean(C_1,100);
```

```
M_tbd_1 = movmean(tbd_1,100);

M_C_3 = movmean(C_3,100);
M_tbd_3 = movmean(tbd_3,100);



%%
%Average of all the individual cases

avg_t_L_1=mean(s_t_L_1);
avg_q_a_1_pre_treatment=mean(s_q_a_1);
avg_t_L_3=mean(s_t_L_3);
avg_q_a_3_pre_treatment=mean(s_q_a_3);


%%Average of q_a in Coulombs when
%the discharges and tbd have been matched
avg_q_a_1=mean(s_q_a_1_pico_tbd*1e-12)
avg_q_a_3=mean(s_q_a_3_pico_tbd*1e-12);


%Average recovery time
avg_t_R_1=mean(s_t_R_1);
avg_t_R_3=mean(s_t_R_3);

%Average time between discharges
avg_s_t_prev_disch_1=mean(s_t_prev_disch_1);
avg_s_t_prev_disch_3=mean(s_t_prev_disch_3);


%% k ratios
k_1_analytical = C_b_1*dV_dt_1; %Based on the theory
k_3_analytical = C_b_3*dV_dt_3; %Based on the theory

k_1=avg_q_a_1/avg_s_t_prev_disch_1 %Based on the prediction model
k_3=avg_q_a_3/avg_s_t_prev_disch_3 %Based on the prediction model

k_total=k_3/k_1



```

```
353 %%Ratios for q_a and tbd
354 ratio_tbd=avg_s_t_prev_disch_3/avg_s_t_prev_disch_1
355
356 ratio_q_a=avg_q_a_3/avg_q_a_1
357
358 %%
```

A.2 High Voltage DC Partial Discharges deterministic prediction model Matlab code

```
%%
clear
close all
clc


format long
%%High Voltage DC Partial Discharges deterministic prediction model

%General considerations

%%Permittivity PET
epsilon_rel=3.1; %PET
epsilon_0=8.8541878176e-12;

%%Conductivity [S/m] and resistivity [Ohm/m] PET
cond=1e-15;
resi=1/cond;

%%Permittivity and conductiviy [S/m] of air
cond_air=5e-50;  %Assuming the conductivity in air is almost zero
                 %so all the votlage drop occurs in the cavity
resi_air=1/cond_air;
epsilon_rel_air=1;

%Heigh of the sample (H) and height of the cavity (h) in [m]
H=250e-6;
h=75e-6;


%%Diameter and Radius of the cavity in the sample in [m]
D_1=0.002;

R_1=D_1/2;

D_3=0.006;
R_3=D_3/2;
```

```
38
39
40 %%Area of the cavity [m^2]
41 A_1=pi*R_1^2;
42 A_3=pi*R_3^2;
43
44 %%Calculating C_b
45 C_b_1=epsilon_rel*epsilon_0*(A_1/(H-h));
46 C_b_3=epsilon_rel*epsilon_0*(A_3/(H-h));
47
48 %Calculating C_c
49 C_c_1=epsilon_rel_air*epsilon_0*(A_1/(h));
50 C_c_3=epsilon_rel_air*epsilon_0*(A_3/(h));
51
52 %Calculating R_c
53 R_c_1=resi_air*((h)/A_1);
54 R_c_3=resi_air*((h)/A_3);
55
56 %Calculating R_b
57 R_b_1=resi*((H-h)/A_1);
58 R_b_3=resi*((H-h)/A_3);
59
60 %%
61 %%The time constant
62
63 tau_1=((R_b_1*R_c_1)*(C_b_1+C_c_1))/(R_b_1+R_c_1);
64 tau_3=((R_b_3*R_c_3)*(C_b_3+C_c_3))/(R_b_3+R_c_3);
65
66
67
68 %%
69 %%V_con (Voltage across the void)
70
71 V_0=10000; %V test voltage
72
73 V_con_1=V_0*(R_c_1/(R_b_1+R_c_1));
74 V_con_3=V_0*(R_c_3/(R_b_1+R_c_3));
75
76 %%V_pasch
77 h_mm=h*1000;
78 p=1*1.01325;
```

```
79
80 V_min=(2420*p*h_mm+2080*sqrt(p*h_mm));
81
82 %%dV/dt
83 V_r=V_min; %For Townsend discharges
84
85 dV_dt_1=(V_con_1-V_r)/tau_1;
86 dV_dt_3=(V_con_3-V_r)/tau_3;
87
88
89
90 %%
91 %%Generating the basic parameters
92 store_t_L_1(1)=0;
93 store_t_L_3(1)=0;
94 index=1;
95
96
97 for count = 1:10000
98
99
100  index=index+1;
101
102 Delta_V_c_1=8.6;      % Extracted from the stochastic model
103                       %in order to make them comparable
104 Delta_V_c_3=Delta_V_c_1;
105
106 % Discharge magnitude
107 q_a_1=C_b_1*Delta_V_c_1;
108 q_a_3=C_b_3*Delta_V_c_3;
109
110
111 %Time between discharges
112 tbd_1=Delta_V_c_1/dV_dt_1;
113 tbd_3=Delta_V_c_3/dV_dt_3;
114
115
116 %Storing the variables
117
118 store_q_a_1(index)=q_a_1;
119 store_q_a_3(index)=q_a_3;
```

```
120 store_tbd_1(index)=tbd_1;
121 store_tbd_3(index)=tbd_3;
122
123 store_index(index)=index;
124
125
126 end
127
128 %%
129 %%Vector treatment
130 length_vec=length(store_q_a_1);
131
132 store_q_a_1;
133 store_q_a_3;
134 store_tbd_1;
135 store_tbd_3;
136
137 s_q_a_1=store_q_a_1(:,3:length_vec);
138 s_q_a_3=store_q_a_3(:,3:length_vec);
139 s_tbd_1=store_tbd_1(:,3:length_vec);
140 s_tbd_3=store_tbd_3(:,3:length_vec);
141
142
143 %%
144 %%Changing units of the stored values.
145 %q_a from [C] to [pC]
146
147 s_q_a_1_pico=s_q_a_1*1e12;
148
149 s_q_a_3_pico=s_q_a_3*1e12;
150
151
152 %%
153 %Creating a time vector to simulate the labratory experiments
154
155 num=length_vec-1;
156 num_1=length_vec-2;
157 num_2=length_vec-3;
158
159 a_1=s_tbd_1;
160 a_3=s_tbd_3;
```

```
pp=1;

for j=2:num

    b_1=a_1(pp);
    b_3=a_3(pp);


    s_b_1(j)=b_1;
    s_b_3(j)=b_3;

    pp=pp+1;
end

s_b_1;
s_b_3;

vv=1;
bb=0;
for g=2:num

    if g<3
    c_1=s_b_1(1)+s_b_1(2);
    c_3=s_b_3(1)+s_b_3(2);

    s_c_1(vv)=c_1;
    s_c_3(vv)=c_3;

    else

     s_c_1(vv)=s_c_1(bb)+s_b_1(g);
     s_c_3(vv)=s_c_3(bb)+s_b_3(g);


    end
    vv=vv+1;
    bb=bb+1;
end

%%s_c is the time of discharges
%organized chornologically
```

```
s_c_1;
s_c_3;

%Vector organisation and treatement
s_c_1_h=s_c_1/(60*60);
s_c_3_h=s_c_3/(60*60);

s_q_a_1_pico;
s_c_1;

s_q_a_3_pico;
s_c_3;


%%
%%Moving average
C_1=s_q_a_1_pico;
tbd_1=s_tbd_1;
t_1=s_c_1_h;

C_3=s_q_a_3_pico;
tbd_3=s_tbd_3;
t_3=s_c_3_h;

M_C_1 = movmean(C_1,100);
M_tbd_1 = movmean(tbd_1,100);

M_C_3 = movmean(C_3,100);
M_tbd_3 = movmean(tbd_3,100);


%%
%Average of all the individual cases


avg_q_a_1=mean(s_q_a_1);
avg_q_a_3=mean(s_q_a_3);

avg_tbd_1=mean(s_tbd_1);
avg_tbd_3=mean(s_tbd_3);

```

```
243
244 %% k ratios
245
246 k_1_analytical = C_b_1*dV_dt_1; %Based on the theory
247 k_3_analytical = C_b_3*dV_dt_3; %Based on the theory
248
249 k_1=avg_q_a_1/avg_tbd_1          %Based on the prediction model
250 k_3=avg_q_a_3/avg_tbd_3          %Based on the prediction model
251
252
253 k_total=k_3/k_1
254
255
256 %%Ratios for q_a and tbd
257 ratio_tbd=avg_tbd_3/avg_tbd_1
258
259 ratio_q_a=avg_q_a_3/avg_q_a_1
260
261 %%
```

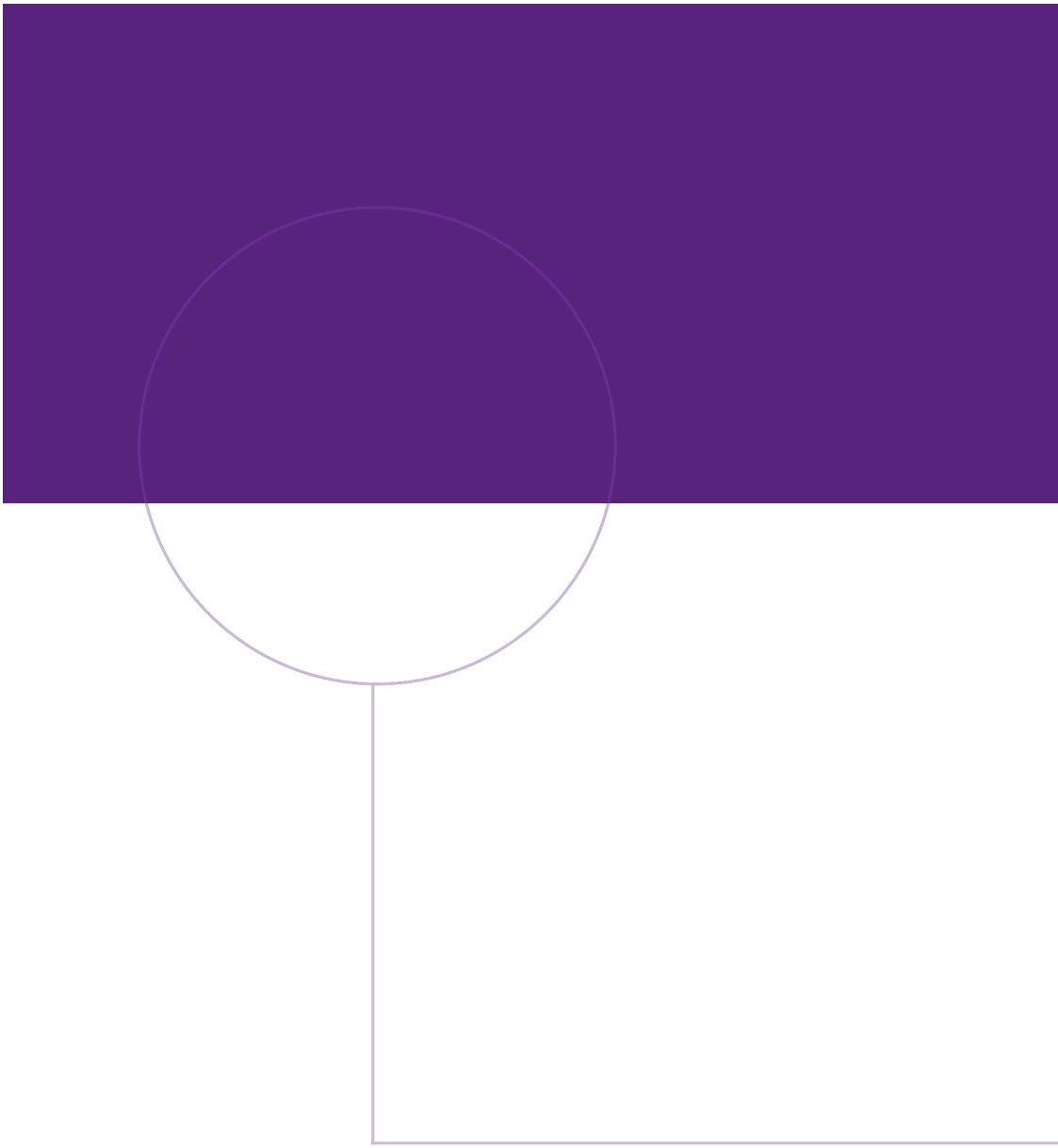

NTNU

Norwegian University of
Science and Technology